REMODELING OF FIBER AND LAMINAR ARCHITECTURE OF RAT HEART

SEPTUM IN A TRANSITIONAL NORMAL STATE BETWEEN PRESSURE

OVERLOAD HYPERTROPHY AND FAILURE

A Dissertation

by

BHARATI KRISHNA HEGDE

Submitted to the Office of Graduate Studies of
Texas A&M University
in partial fulfillment of the requirements for the degree of

DOCTOR OF PHILOSOPHY

August 2006

Major Subject: Biomedical Engineering

REMODELING OF FIBER AND LAMINAR ARCHITECTURE OF RAT HEART

SEPTUM IN A TRANSITIONAL NORMAL STATE BETWEEN PRESSURE

OVERLOAD HYPERTROPHY AND FAILURE

A Dissertation

by

BHARATI KRISHNA HEGDE

Submitted to the Office of Graduate Studies of
Texas A&M University
in partial fulfillment of the requirements for the degree of

DOCTOR OF PHILOSOPHY

Approved by:

Chair of Committee,	John Criscione
Committee Members,	Christopher Quick
	Hsin-i Wu
	William Hyman
Head of Department,	Gerard Cote

August 2006

Major Subject: Biomedical Engineering

ABSTRACT

Remodeling of Fiber and Laminar Architecture of Rat Heart Septum in a

Transitional Normal State Between Pressure Overload Hypertrophy and Failure.

(August 2006)

Bharati Krishna Hegde, B.E., University of Pune, India;

M.S., Texas A&M University

Chair of Advisory Committee: Dr. John Criscione

Congestive Heart Failure (CHF) is a major fatal disease today in the United States. The heart's function is a mechanical one. To diagnose and treat CHF effectively there is a need to understand at the microstructural level, the differences in the response of the myocardium to a change in its mechanical environment. Hence to assess growth and remodeling processes in the myocardium, the fiber and myolaminar structure of two groups of Dahl salt-sensitive rats were compared: low salt (LS) normal controls and a high salt (HS) group with hearts in "transitional eutrophy" defined by normal size and shape but in transition from pressure overload hypertrophy to dilated hypertrophy. To create the HS group with transitional eutrophy, we fed Dahl salt-sensitive rats, a sustained high salt diet from age 6 wks till sacrifice at age 11-13 wks. Such rats have a heart that transitions from too thick (pressure overload hypertrophy at about age 9 wks) to too thin (dilated hypertrophy at about age 15 wks to death) with a transitional period (age 11-13 wks) having normal size and shape. Fiber angles, sheet angles, number and thickness of sheets were measured in the septum at four transmural quarters (TQ1 to TQ4 with TQ1 being closest to LV and TQ4 closest to RV). A uniformity index was defined to characterize sheet angle dispersion. Upon comparison to LS controls, the HS group had normal size

hearts with normal shape. However, there was a significant increase in the number of sheets, which corresponded with a significant decrease in the thickness of sheets in all quarters in HS group. Differences in fiber angles were significant in TQ1, TQ2, and TQ4 with fiber angles more positive in HS group. Differences in sheet angles and uniformity index were not significant. Despite having a normal size and shape, we found that hearts in a state of transitional eutrophy have a significantly different fiber and sheet morphology.

The experimental data was used to develop a model that represents the path to failure that may be taken by the myolaminae when the heart is subjected to excessive pressure overload.

To my beloved parents

ACKNOWLEDGEMENTS

TABLE OF CONTENTS

LIST OF TABLES

LIST OF FIGURES

FIGURE   Page

FIGURE

Page

CHAPTER I

INTRODUCTION

A.   Motivation

Congestive heart failure (CHF) is a chronic disorder in which the heart is unable to pump sufficient amounts of blood to meet the body's metabolic needs. Approximately 5 million people in America suffer from this disease and around 550,000 new cases are diagnosed every year. Most instances of CHF are thought to be caused due to progressive deterioration of the myocardial contractile function. This could be brought about by ischemic injury, pressure or volume overload or dilated cardiomyopathy (19). It is known that the heart grows and remodels in health (exercise hypertrophy) and disease (volume and pressure overload hypertrophy). The mechanical nature of the heart makes it important to understand how and why the myocardium responds to its normal as well as changed mechanical environment. This is the logical first step in the diagnosis and treatment of this killer disease. This work deals with the quantitative histological investigation of the normal versus diseased rat heart septum. The results of this investigation are used to build a growth model which will provide better insight into our understanding of the mechanics of normal versus diseased hearts.

Ever since Streeter (62) quantified that there is a smooth transmural variation of fiber orientation through the heart wall, there have been many studies done on myocardial fiber orientation. Ventricular myocardium consists of a complex three-dimensional structure that has been inferred previously from two-dimensional images. For years many researchers have been involved (62, 44, 34, 71) in working on quantifying the microstructure. However, most studies mapped the muscle fiber orientation

The journal model is *AJP-Heart and Circulatory Physiology.*

at a limited number of ventricular sites and the fiber architecture was never quantitatively referred to ventricular geometry. Hence, the data obtained proved to be a more qualitative rather than a quantitative description of the cardiac fiber distribution within the myocardium.

Most histological investigations of the myocardium single out each of its constituents viz. collagen, myocytes etc. But, the myocardium functions as a composite structure. It is made up of sheet-like structures called myolaminae. A myolamina consists of 3-4 myocytes stacked together and surrounded by a weave of collagen. The gaps between the myolaminae are called the cleavage planes. Over the years, the functional importance of the laminar organization of the myocardium has been well-discussed.

As discussed in (42), there is no gross anatomical evidence of a sheet structure or radial septation. The sheet structure is local rather than global. With a narrow field of view and high magnification, myocardial structure is sheet-like or laminar; yet with a wide field of view and low magnification, the sheets appear as small gaps with no overall or global laminar structure. This laminar structure, though only evident locally, is thought to have a global function of contributing to ventricular wall thickening via large cross-fiber strains as shown in previous studies (18, 36, 21).

Fiber orientation is also thought to be an important parameter in the determination of myocardial stress and strain (36, 67). Studies on myocardial deformation have also provided evidence to support the idea that cleavage planes in the myocardium re-arrange muscle fiber bundles to accommodate wall thickness changes through the shearing deformation between the myocardial laminae (36, 67, 61). The slippage of the adjacent myofiber bundles along the cleavage planes between the sheets is also thought to be responsible for ventricular cavity dimension changes and changes in wall thickness (61, 14). Thus, the myocardial fiber and laminar structures play an impor-

tant role in normal LV contraction and relaxation during the cardiac cycle. However, the mechanistic significance of the fiber and laminar structures due to growth and remodeling in the various hypertrophies and infarct regions remains unknown.

Currently there is a need for a quantitative study of the myocardium that can integrate the histological data obtained from experiments along with a growth model that helps explain changes that the myolaminae undergo as the heart progresses to failure. To understand the fundamental differences between the normal and diseased conditions of the heart, a comparative study followed by a model that incorporates both types of data is the need of the hour and will help bring more insight into the study of the growth and remodeling of the heart. Hence, this work aims to fill this knowledge gap by integration of experiment data (normal versus hypertrophied) followed by a growth model. This will shed light on the microstructural differences between the normal and diseased hearts and also identify the path taken by the myolaminae as they transition to failure.

B. Literature Survey for Experimental Design

Significant amount of work has been done in the past to understand better the mechanics of the fiber and laminar structure of the heart. This section summarizes some papers that are relevant to our topic of research.

LeGrice et al. (34) drew up a mathematical model to describe the cardiac anatomy of arrested dog heart. Their model can be used with finite element models of electrical activation and mechanical function of the heart. Their main contribution was defining the axes of material symmetry that reflects the local structure of the ventricular myocardium. In their model, the cardiac microstructure is assumed to have three axes of symmetry: one aligned with the muscle fiber orientation (the fiber

axis), a second set orthogonal to the plane (sheet axis), and a third set orthogonal to the first two, the sheet-normal direction. This is a rather realistic description of the local structural anisotropy of the myocardium which facilitates use of this model in the continuum analysis of cardiac function.

Young et al. (71) developed a technique for imaging the 3D microstructure of rat heart in conjunction with the collagen network in extended blocks of myocardium, using confocal laser microscopy. In their method, entire tissue blocks were imaged, one "slice mosaic" (a set of slices at the same z location) at a time. In order to do this, the tissue block was imaged at multiple depths. The block was then removed, sliced down to 40 μm, replaced and imaged at new depths. They clearly demonstrated the laminar organization of myocytes and the extensive cleavage planes between the layers using a detailed technique for tissue processing and 3D visualization. Yet, their procedure is a very time consuming process, produces a large amount of data and hence requires large amount of computer memory.

Costa et al. (18) demonstrated that normal LV mechanics involve considerable deformation of laminar sheets of myocardium. In the anterior LV free wall, the sheets become thinner from end diastole to end systole and there is substantial sheet extension transverse to the muscle fibers that varies transmurally and regionally. They also showed that there are regional differences in the 3-D laminar architecture. Both LeGrice et al. (34) and Costa et al. (18) observed that in certain regions of the ventricular wall of canine hearts, myocardial sheets contribute to systolic wall thickening mainly via cross-fiber sheet shear and sheet extension.

Dou et al. (21) found in their study of human heart using MRI that in addition to the above two cross-fiber terms, sheet-normal thickening also contributed significantly to radial wall thickening near the RV. They also showed that sheet shear is the preferred method for systolic wall thickening in humans. They proposed that sheet

extension may be the result of the sum of the increased diameter of myocytes due to the fiber shortening and a mechanical stretching-apart of the myocytes along the sheet direction. They also found that fibers become more longitudinally oriented during systole. In both human and canine studies (34, 18, 21) it was found that sheets preferred to slide relative to one another along the sheet direction rather than the fiber direction as reflected by the large sheet normal shear and small fiber normal shear observed in both studies.

Spotnitz et al. (61) showed that an increase in wall thickness was associated with decreased sheet slope and increased number of fibers across the wall rather than an increase in fiber size.

Takayama et al. (64) and Dou et al. (21) suggested that during diastole when the wall thins, the three major sheet strains: sheet extension, sheet shear and sheet normal thickening, reverse relative to those of systole. Takayama et al. (64) found that during diastole, sheets shorten and rotate away from radial direction which is opposite of what happens in systole.

Chen et al. (15) found that changes in sheet and fiber orientation provide a substantial mechanism for radial wall thickening independent of active components due to myofiber shortening. In other words, they proposed that myocyte contraction contributes to radial wall thickening and ventricular ejection both by myocyte shortening and by the related secondary induction of changes in fiber and sheet organization.

Zimmerman et al. (72) showed that in the three weeks following myocardial infarction in pig, noninfarcted tissue adjacent to the infarct remodeled by expansion along the direction of fibers and cross-fibers. They showed that these changes are induced due to myocyte elongation, myofiber re-arrangement (cell slippage) as well as a change in cell shape to an elliptical cross-section with major axis in the epicardial tangent plane. There was a significant positive cross-fiber remodeling strain which

could be explained by rotation of myocytes or alterations in the orientation of the laminar architecture. The inner half of the ventricular wall adjacent to the myocardial infarction thinned substantially which could be due to cell slippage or change in myocyte shape to a flatter cell. This was one of the first groups to demonstrate cross-fiber remodeling.

Ashikaga et al. (10) determined the 3-D finite deformation in the LV anterior wall during early relaxation in normal dog hearts in vivo. Their strain analysis indicated rather complex fiber and sheet mechanics with transmural heterogeneity during early relaxation represented by myofiber stretch in the epicardial layers, which confirms modeling predictions of a predominant role of epicardial fibers and sheet shortening transverse to the fibers in the endocardial layers, all of which may aid early diastolic filling.

Using the data of Costa et al. (18), Arts et al. (9) tested the hypothesis that sheets are oriented along the planes of maximum shear subject to the constraint that they also contain the myofiber axis. With this hypothesis two distinct populations of sheet orientation were found, often with similar probability. When pooling experimental data, both the populations were evident and showed close agreement with the simulated directions.

Harrington et al. (29) sought to characterize transmural sheet orientations in ovine anterolateral LV wall. They excised 1 mm thick sections of myocardial tissue parallel to the epicardial tangent plane from the epicardium to the endocardium. They identified two families of sheet angles: +45 degrees (β^+) and -45 degrees (β^-). In the equatorial region near the epicardium, sheets belonged to β^+ family, in the midwall to the β^- family and near the endocardium to the β^+ family. In the basal region, the trend was reversed. They believed that their data created an "accordion-like" wall thickening mechanism which may facilitate wall thickening via laminar shear

in the ventricle. This laminar distribution allows alternating shear to occur within the wall such that there is minimal shear displacement of the epicardium relative to the endocardium. In this study, the thickness of the slices was 1 mm. Much thinner slices would have given a different result probably, one that is a better representation of the true laminar architecture. Also, they have focussed on only the basal and equatorial regions of the LV walls. It has been previously shown ((18, 64, 35)) that there is a variation in sheet angle distribution from apex to base. Hence their results should be extrapolated with caution to other regions of the LV wall.

Recent work in our laboratory has resulted in the development of a time and cost efficient, faster processing method for histological investigation of rat hearts. This method preserves the orientation of the fiber and sheet structure and can be used for multiple hearts in an efficient manner. In this method, plastic tissue embedding was used as opposed to paraffin embedding which grossly distorts the tissue structure.

1. The Compensated States of Overload

Grossman et al. (27) proposed the theory that when the primary stimulus to hypertrophy is LV **pressure overload**, there is an increase in the peak systolic wall stress leading to a parallel replication of sarcomeres, resulting in wall thickening and **concentric hypertrophy**. The wall thickening serves to return the peak systolic stress back to normal. On the other hand, if the primary stimulus is **volume overload**, the increased end diastolic stress leads to a series replication of sarcomeres, fiber elongation, chamber enlargement and **eccentric hypertrophy**. This chamber enlargement leads to increased systolic stress which then causes wall thickening, sufficient enough to normalize the systolic stress. Volume overload hypertrophied patients show considerable increases in both chamber and wall thickness so their thickness to radius ratio is almost normal. Thus the pressure-overloaded hearts exhibit concentric hypertro-

phy with increased thickness-to-radius ratio, normal peak systolic and end-diastolic wall stresses while volume overloaded hearts exhibit eccentric hypertrophy with an increased diameter but normal thickness to radius ratio, normal peak systolic wall stress and increased end-diastolic wall stress. Figure 1 shows the adaptations of the heart to the two different kinds of stimuli: pressure and volume overload. Excessive overload of either kind leads to chamber dilation, wall thinning and an irreversible condition leading to heart failure. The duration of compensation varies from weeks in rodents to months or even years in humans.

C. Research Objectives

Based on the literature available on the study of the rat heart microstructure it is seen that although there have been previous studies in this area there is a lack of a comparative quantitative study of the detailed histology of normal hearts versus hearts progressing towards congestive heart failure. Also, there is a need to tie together the experimental work with a model to understand better how the heart transitions from the normal to the diseased state. Hence, the objectives of this study are listed as under:

1. To perform a detailed histological investigation of the microstructure of normal rat heart septae and rat heart septae progressing toward heart failure. The analysis should involve fiber and sheet structure analysis of both the normal and the diseased hearts and a comparative analysis of both.

2. To build a growth model using the data obtained from the histological study which will the changes in the sheet structure as the heart progresses to failure.

A. Normal LV Cross-Section

B. Concentric Hypertrophy due to Pressure Overload

R

T

R

T

R

T

C. Eccentric Hypertrophy due to Volume Overload

T: Wall Thickness; R: Radius
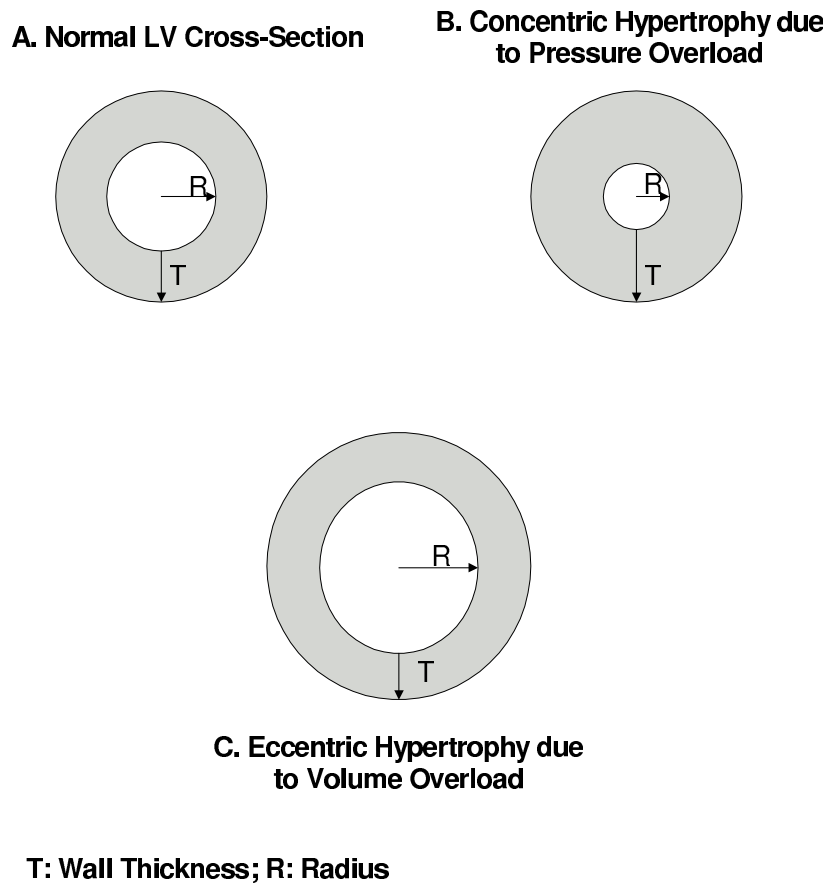
Fig. 1. The Compensated States of Overload; Note: A. Normal Heart; B. Pressure Overloaded Heart; C. Volume Overloaded Heart; The thickness to radius ratio in the concentric hypertrophy state increases as opposed to the decrease in the thickness to radius ratio in the eccentric hypertrophy state

D.   Methods

1.   Histological Investigation

Eleven Dahl salt-sensitive rats were fed a low-salt diet to form the LS group of rats. Ten more rats of the same type were fed a high-salt diet from age 6 wks till sacrifice at age 11-13 wks to create a HS group of hearts in a state of transitional eutrophy. "Transitional Eutrophy" is a term that we use to define the heart stage with normal size and shape but transitioning from pressure-overload (concentric) hypertrophy to dilated hypertrophy. The septae of the rat hearts were sliced and imaged at the original thickness, midsection, one-fourth and three-fourth of the original thickness using a recently developed, fast and effective slicing method ("E.H. Jetton, unpublished observation"). Fiber angles were calculated for both the rat groups. To calculate the myolaminar sheet angles, the slices were placed in the infiltrating solution for a week after which they were cut in the cross-fiber direction and placed in molds filled with hardening solution for a week until they were hardened appropriately. Following this, they were sliced at 10μm thickness using a microtome. The four depths of the septae were called transmural quarters and represented as TQ:

1. TQ1: The septal wall closest to the LV side was called TQ1.

2. TQ2: The septal mid-wall closer to the LV side was called TQ2.

3. TQ3: The septal mid-wall closer to the RV side was called TQ3.

4. TQ4: The septal wall closest to the RV side was called TQ4.

Sheet angles, total number of sheets, uniformity index and thickness of the sheets was measured at each quarter of the septum. Comparison between these parameters in both the groups was made.

2.   Growth Model

Using data from the histological investigation, a growth model of the heart was built. This model depicts the path taken by the myolaminae as the heart transitions from pressure-overload hypertrophy to dilated hypertrophy on its way to heart failure, using the data obtained from this study.

E.   Anticipated Contributions of This Research

Although present treatments are continuously improving, there are many things that we do not fully understand about the mechanics of cardiac growth and remodeling. Past researchers have found that altered hemodynamic loading and/or heart disease leads to growth and remodeling of myocytes and extracellular matrix (26). Also, myocytes and cardiac fibroblasts are highly mechanosensitive in the sense that even subtle mechanical stimuli can influence gene expression. Therefore it is possible and likely that mechanical stress or strain can control growth, orientation and differentiation of contractile dysfunction of myocytes (49).

Studies of growth and remodeling in cardiac hypertrophy are difficult because it is a great challenge to account for the many changing variables (i.e., after load, preload, heart size, heart shape, blood chemistry, nerve and hormonal control, etc.). The significance or power of our study of remodeling is the fact that heart size and shape are normal in the HS group. The analysis of healthy hearts versus hearts transitioning to failure is essential to define the transmural heterogeneities in the material properties. A thorough knowledge of the differences in the microstructure of the two states will help the development of new and more effective treatment methodologies.

Through this study, we intend to improve our understanding of the histology as

well as mechanics of the healthy heart as compared to a heart transitioning to congestive heart failure. The anticipated contributions of this research can be summarized as follows:

1. Quantification of the detailed microstructure of multiple healthy hearts versus hearts in transition to failure using a fast and efficient processing method.

2. A growth model based on the above data that will help depict the path travelled by the myolaminae as the overloaded heart transitions to failure when subjected to excessive pressure overload.

F.   Organization of Dissertation

Chapter II of the dissertation deals with background about the structure of mammalian heart, structure of the myocardium and some basics of heart failure. Chapter III discusses the experimental methods that were used to delineate the fiber and sheet structure. The results of the histological experiments are presented in detail in Chapter IV. Chapter V presents the growth model that describes the path taken by the myolaminae as the heart transitions from pressure overload hypertrophy to failure. Chapter VI summarizes the findings of our study.

CHAPTER II

BACKGROUND AND SIGNIFICANCE

Much of the descriptions of the human heart, myocardium and myocyte structures in this chapter have been adapted and paraphrased from Levick (37).

A.   Structure of the Human Heart

The heart is a compact muscular pump which contracts nearly 2.5 billion times during the human life span (31). The human heart is a cone-shaped, four-chambered hollow muscle, 12 cm long by 9 cm wide. It consists of two intermittent muscular pumps, the right and the left ventricles (37). The left and the right atria are thin-walled low pressure contractile reservoirs that fill the respective ventricles. Deoxygenated blood returns to the right atrium via the two great veins, the superior vena cava and inferior vena cava and is sent to the right ventricle. This blood is then pumped out from the right ventricle and sent to the lungs to become oxygenated through the pulmonary artery. Pulmonary veins return the oxygenated blood from the lungs to the left atrium which sends it to the left ventricle. The left ventricle pumps out the same volume of oxygenated blood through the aorta to the rest of the body.

The four chambers are built around a ring of fibrous tissue called the annulus fibrosus which is situated at the atrioventricular junction. This region which barely moves at all is called the base of the heart. The bottom tip of the heart which moves substantially during contraction is called the apex (37). Unlike the atria, the ventricles are formed by a continuum of muscle fibers that start from the fibrous skeleton at the base of the heart and sweep up toward the apex at the epicardial surface. While passing toward the endocardium, they gradually undergo a 180-degree change in direction to lie parallel to the epicardial fibers and form the endocardium

and papillary muscles. These fibers twist and turn inward at the apex to form the papillary muscles while at the base they form a thicker muscle that decreases the ventricular circumference during the ejection of blood. In addition to this reduction in circumference, ventricular ejection is also accomplished with a decrease in the longitudinal axis due to the descent of the base of the heart (12). The entire heart is enclosed in a fibrous sac called the pericardium. The wall of the heart is made up of three distinct layers: the outer, inner and middle layers called the epicardium, endocardium and myocardium respectively. The epicardium is a thin serous layer about 100 μm thick consisting largely of a two-dimensional plexus of collagen and some elastic fibers. The endocardium is also about 100μm thick and lines the insides of each cardiac chamber. The myocardium or parenchymal tissue is the functional or working tissue of the heart that allows it to pump blood.

1.   Structure of Myocardium

It is currently accepted that the ventricular myocardium is a continuum composed of myofibers that vary smoothly in direction as they move from the epicardium to the endocardium (35). The laminar structured myocardium contains sheets of strongly coupled fibers separated by gaps called cleavage planes. These sheets (also called myolaminae), which are about four cells (myocytes) thick, surrounded by collagen, and directed radially across the ventricle, continually branch and interconnect both across and around the wall to form a strongly integrated three-dimensional structure with three axes of material symmetry at each point in the myocardium (36).

Since the myocardium is the working tissue of the heart, problems with the functioning of the heart would directly relate to problems with the functioning of the cells of the myocardium which actually help carry out the work of the myocardium i.e. the myocytes. Cardiac myocytes constitute one-third of all cells found in the

myocardial tissue; the remainder include fibroblasts, endothelial and vascular smooth muscle cells (68). It would be worthwhile at this point to have a look at the structural compostion of the myocyte.

2. Structure of the Myocyte

Myocytes are arranged into locally parallel muscle fibers which in turn are embedded in an extracellular matrix consisting largely of type I and type II collagen. The orientation of these muscle fibers change with position in the wall of the heart (31). The following description of the myocyte structure has been paraphrased from Levick (37). The human myocyte is 10-20 μm in diameter by 50-100 μm long. It is sometimes branched and contains a single nucleus. Adjacent myocytes are attached end-to-end by a stepped junction called the intercalated disc which has two subsets: gap junction and desmosome. Gap junctions transmit electrical excitation from one myocyte to the other. Gap junction is made up of the protein connexin. Desmosomes serve to rivet the cells together and consist of plaques of cadherin molecules. Each myocyte consists of contractile bundles of diameter approximately 1 μm called myofibrils. Each myofibril is composed of units called sarcomeres joined end-to-end. The sarcomere comprises a set of filamentous proteins between two Z lines which are made up of the protein alpha-actinin. Between the Z lines are two kinds of filaments: thick filaments made up of the protein myosin and thin filaments composed primarily of actin. The thick myosin filaments lie in parallel in the center of the sarcomere. This region is called the A band. The thin filaments lie interposed between the thick filaments. One end of the thin filament is free in the A band and the other end is fixed to the Z line forming the I band. The contraction of the heart is brought about by shortening of the sarcomere by the sliding filament mechanism, the thin filaments slide into the spaces between the thick filaments of the A band (37).

3.   Heart Failure

Heart Failure is a complex syndrome that consists not only of cardiac dysfunction but also of other metabolic and neuro humoral alterations (32). CHF is one of the major fatal diseases in America. The New York Heart Association method of assessment of heart failure classifies it into four stages:

1. Stage 1: diseased but asymptomatic

2. Stage 2: slight limitation of physical activity

3. Stage 3: marked limitation of physical activity

4. Stage 4: inability to do any physical activity, may have angina even at rest.

There are numerous factors that contribute to and eventually culminate in CHF. According to Cotran et al. (19), some of these mechanisms include:

1. Obstruction to flow: This occurs during aortic valvular stenosis, systemic hypertension or aortic coarctation causig increase in ventricular chamber pressure. This is the method that we have used in our experimental procedure to induce hypertrophy in the high salt diet rats. The heart is subjected to various stages of overload before it eventually succumbs to CHF as depicted in Figure 2.

2. Regurgitant flow: Mitral or aortic valve regurgitation causes backward reflux of blood after each contraction causing excessive volume overload on the ventricle. The stages involved in this process are depicted in Figure 3.

3. Failure of the pump: The cardiac muscle may be damaged resulting in inadequate contraction and disability of chambers to empty properly. Valvular heart disease, coronary artery disease, congenital heart disease are some causes of pump failure.

4. Cardiac conduction problems that occur due to ventricular fibrillation, arrythmias, heart blocks etc.

Normal LV Cross-section

Concentric Hypertrophy

Pressure
Overload

R

T

R

T

R

T

Further
Pressure
Overload

**Dilated
Hypertrophy
Culminating in
CHF**

R

T

R

T

T: Wall Thickness; R: Radius
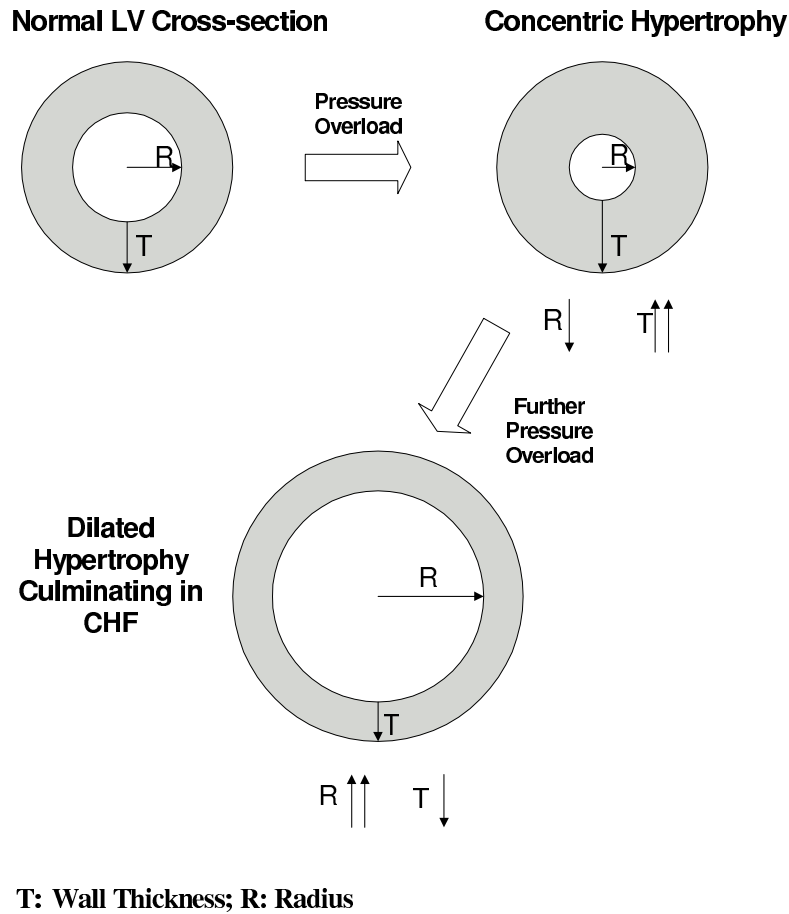
Fig. 2. CHF Caused by Pressure Overload (Aortic Stenosis or Hypertension)

CHF is divided into three categories: Left heart failure, right heart failure and high output failure. Left heart failure, which is the most common type of failure is further divided into systolic heart failure and diastolic heart failure. Systolic heart failure is defined as the inability of the heart to generate adequate cardiac output to perfuse the vital organs. Diastolic heart failure is defined as pulmonary congestion despite a normal stroke volume and cardiac output. Both types of failure stem

Normal LV Cross-section

Eccentric Hypertrophy

Volume
Overload

R

T

R

T

$R\uparrow$ $T\downarrow$

Further
Volume
Overload

**Dilated
Hypertrophy
Culminating in
CHF**

R

T

$R\uparrow\uparrow$ $T\downarrow$

T: Wall Thickness; R: Radius
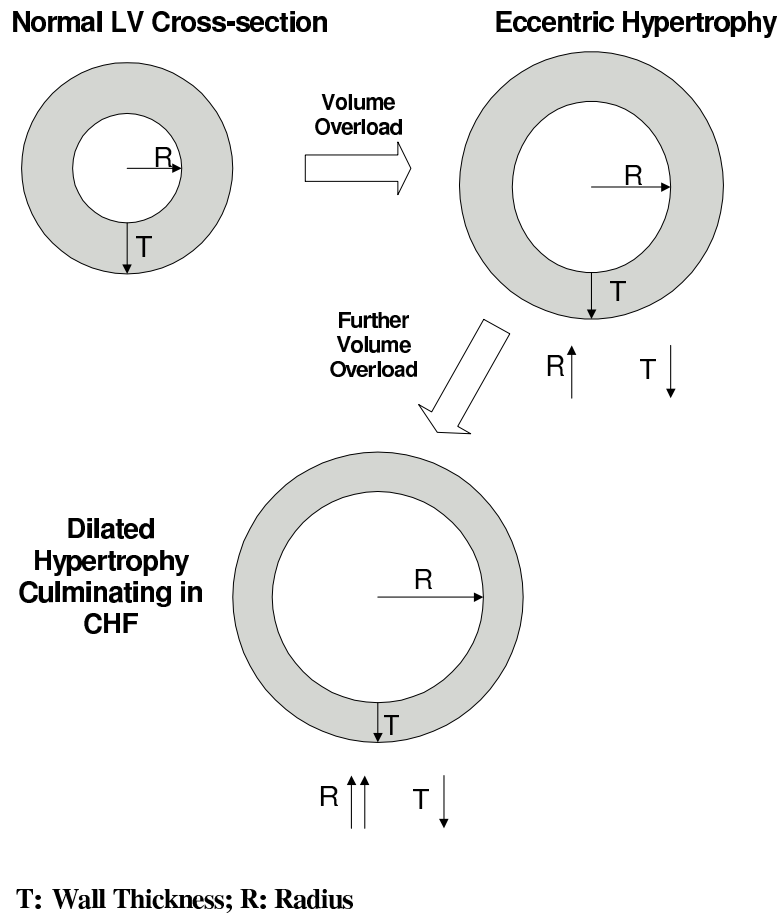
Fig. 3. CHF Caused by Volume Overload (Mitral or Aortic Valve Regurgitation)

from decrease in compliance of heart tissue leading to reduction in contractility. Reduction in contractility stems from disrupted myocyte activity caused by myocardial infarction (most common), myocarditis and cardiomyopathies. Due to this decrease in contractility, there is a decrease in stroke volume and increase in preload causing ventricular remodeling. Figure 4 shows the P-V loops for the normal heart versus a heart that is progressing towards CHF. The decrease in contractility with respect to the control loop is clearly evident.
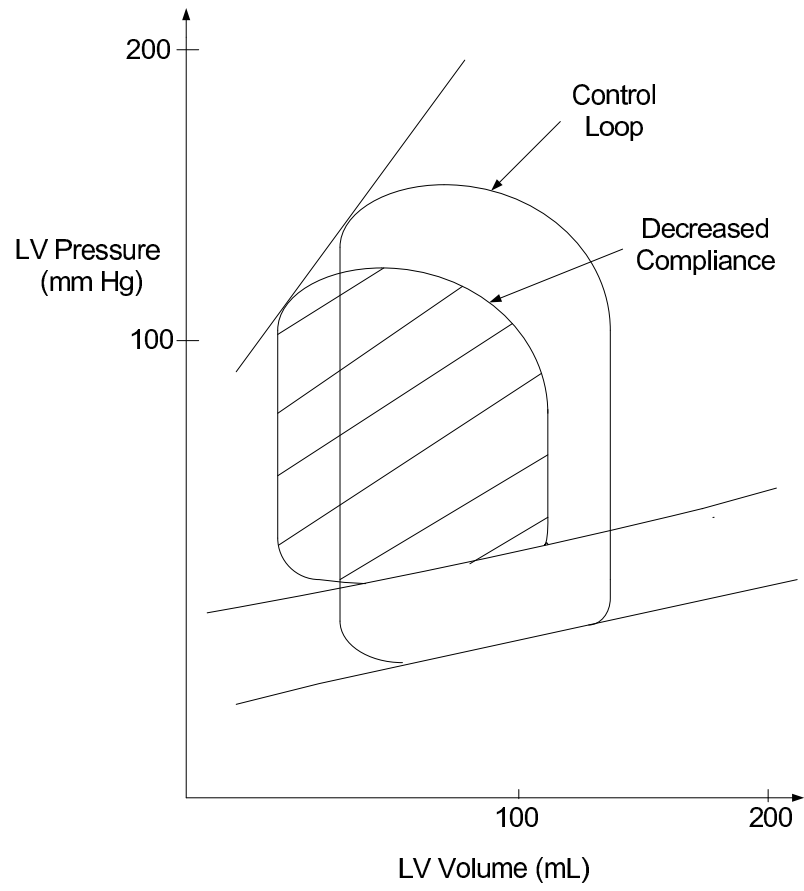
Fig. 4. Pressure Volume Loops

CHAPTER III

MATERIALS AND METHODS

A.   Experimental Design Overview

1.   Interventricular Septum

The interventricular septum is a block of tissue that separates the left ventricle and the right ventricle. The excised septum is nearly planar with uniform thickness such that a simple coordinate system can be used to reconstruct the three-dimensional microstructure from histological sections. There are no papillaries or trabeculae on the LV side of the septum and few trabeculae and small papillaries on the RV side. Therefore, the LV and RV surfaces of the septal wall are fairly well delineated by smooth endocardial membranes and there are no trabeculae-carne-interfaces to cause fiber dispersion (62). As a result, the myofibers in the septum are nearly parallel to the plane of the wall. Therefore, tissue sections parallel to the wall are parallel to the myofiber as well. On the other hand, the LV freewall has large papillaries, much curvature, dramatic changes in wall thickness, and much more fiber dispersion. Since this research investigated the transmural variations in myolaminate morphology and remodeling, the unnecessary complexities of the LV freewall were appropriately avoided.

2.   Animal Model for Hypertrophy

Aortic banding (53, 60), renal artery constriction (13) and coronary artery ligation (41, 52) are common procedures used to create animal models for left ventricle hypertrophy or failure. However these methods have disadvantages of using specific surgical procedures and of having extremely variable time courses in developing heart

failure. Inoko et al. (32) established the Dahl salt-sensitive rat fed a high salt diet as a useful model showing rapidly developing congestive heart failure in which the transition from compensatory hypertrophy to decompensatory dilation of the left ventricle is easily manifested. For our study we used this particular animal model to induce hypertrophy in the rats.

This study dealt with investigating the microstructure of normal versus hypertrophied hearts. Hence, we decided to study the transmural variations in the fiber and sheet structure of normal versus hypertrophied hearts at four depths across the septal wall. Dahl salt-sensitive male Sprague Dawley rats were purchased for the study. Animals were handled and sacrificed under the guidelines of an active animal use protocol in compliance with the rules and regulations of the Texas A&M University System. The low salt (LS) control group (n=11) consisted of rats fed a low salt diet (3% NaCl). The high salt group (HS) (n=10) consisted of rats fed a high salt diet (8% NaCl) from the age of 6 weeks up to 11-13 weeks of age. As discussed in (32), such rats develop hypertrophy at age 9-10 weeks and then transition to dilated hypertrophy at around 15 weeks and die by age 18 weeks.

B. Heart Removal and Fixing Technique

Rats were euthanized using CO_2 inhalation followed by bilateral thoracotomy. The body weights of the rats were measured. An 8-10 mL bolus of 10 mM potassium chloride (KCl), (OmniPur, EMD Chemicals, Gibbstown, NJ) in phosphate buffered solution (PBS 10X, diluted to 1X) (OmniPur, EMD Chemicals, Gibbstown, NJ) was injected rapidly into the LV via a 21 gage needle inserted through the apex of the heart, causing cessation of myocardial activity. The heart was then excised, weighed, and placed in the PBS solution. The left and right atria were removed so that a small

but oversized polyethylene balloon could be placed in the LV cavity and pressurized to 1 kPa (10 cm H_2O). It was important that the balloon was oversized so that there was no tension in the polyethylene whereby the balloon pressure is counterbalanced by a pressure-like normal force on the LV cavity interface. The heart was fixed in formalin for 15 minutes in this definite state of relaxation with 1 kPa filling pressure (end-diastolic state). The balloon was removed and the heart was placed back in formalin for a week to complete fixation.

After fixation, the right ventricle was removed and the diameter of the left ventricle was measured from the posterior to anterior side and the left to right side. The interventricular septum was removed and sliced down to 5 mm in the circumferential direction and 11 mm in the longitudinal direction to fit into the slicing apparatus. The interventricular septum thickness was measured. A right handed cardiac Cartesian system was used to define the cardiac axes for the block of tissue. e_1 was defined to be the circumferential direction pointing towards anterior LV side, e_2 was defined to be the longitudinal direction pointing towards LV base and e_3 was defined to be the radial direction pointing from LV to RV.

C. Tissue Processing for Quantitative Histology

The slicing device as seen in Figure 5 was designed for slicing tissue samples smoothly and evenly in a quick and efficient manner Figure 6 shows an actual photograph of the slicing device. The four depths of the septal wall were called transmural quarters (TQ) and are illustrated in Figure 7. The slicing procedure which revealed these four depths is illustrated in Figure 8. TQ1 was the wall closest to the LV, TQ2 was the mid-wall closer to LV, TQ3 was the mid-wall closer to RV side and TQ4 was the wall closest to RV.
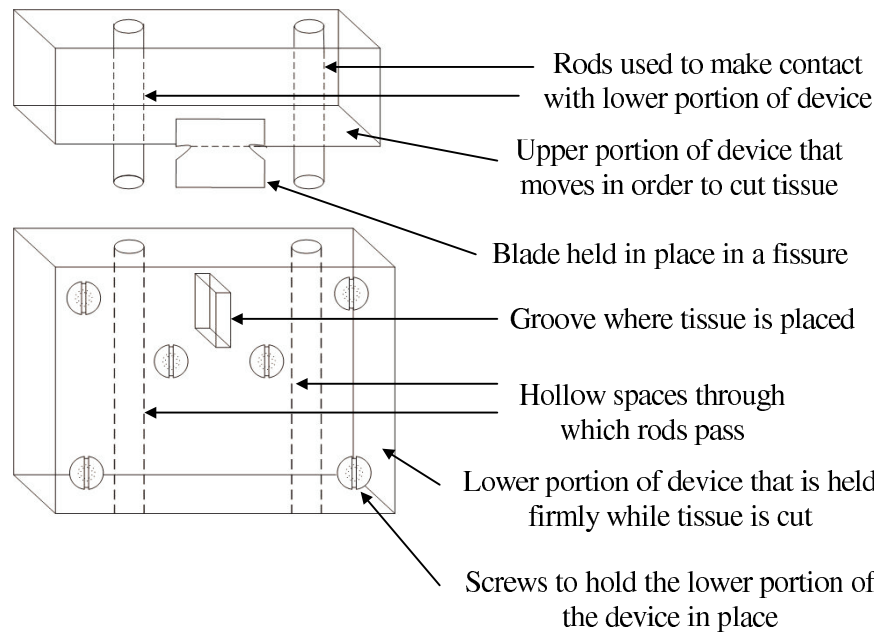
Fig. 5. Slicing Device Illustration
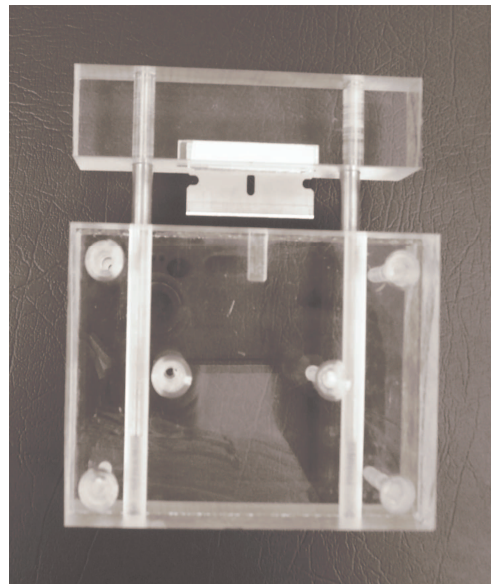
Fig. 6. Slicing Device Photograph
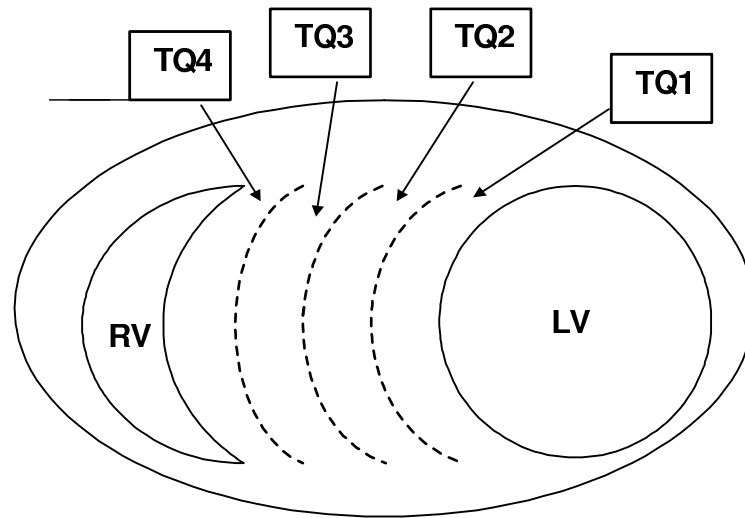
Fig. 7. Illustration of Depths of the Inter-ventricular Septum in an Anterior View of Rat Heart Cross-section; Note: TQ1, TQ2, TQ3 and TQ4 correspond to the four quarters of the septum; LV: Left Ventricle and RV: Right Ventricle; The septum has been enlarged for illustrative purposes

A. SEPTUM BEFORE SLICING

RV Endocardium

Third Cut--75% Original Thickness

First Cut--50% Original Thickness

Second Cut--25% Original Thickness

e_2

e_3

e_1

LV Endocardium

B. SEPTUM AFTER SLICING

TQ1

TQ2

TQ3

TQ4

RV Endocardium

Suture

LV Endocardium
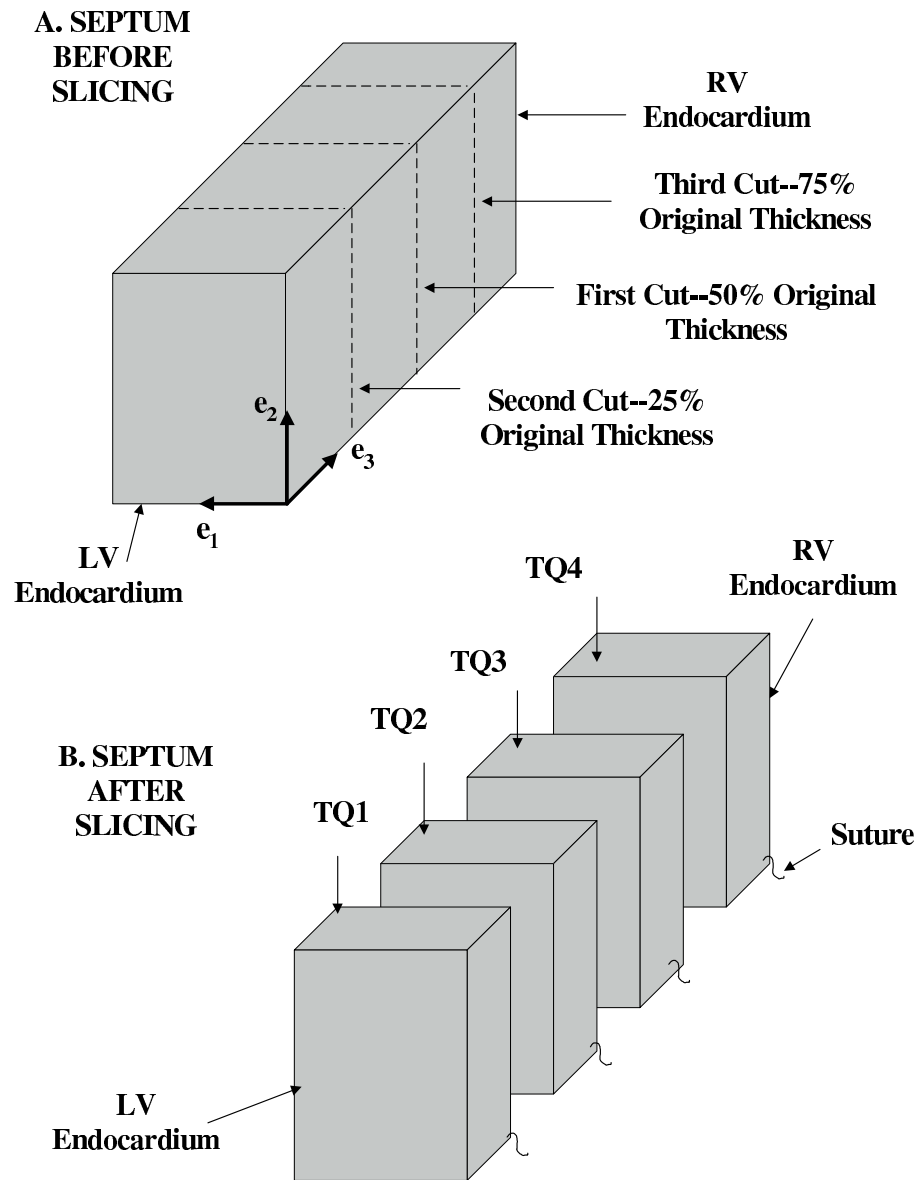
Fig. 8. Illustration of the Slicing Process; Note: A. Block Of Tissue Excised from Interventricular Septum; e_1, e_2, e_3 correspond to the local circumferential, longitudinal and radial axes respectively; B. Blocks of tissue after slicing process is completed

D.   Fiber Angle Measurement

Fiber Angle *"α"* is the angle subtended by the myofiber axis (e_f) to the positive circumferential direction (e_1), α being negative for a left-handed helix system (29). The fiber angle α was measured counterclockwise with respect to the positive circumferential direction as seen in Figure 9B. First, the septum was imaged at the TQ1 (face 1) via light microscopy and α was recorded at 10 locations on this face using Image J, an image processing software (Refer to Figure 9A for a description of the faces and quarters in the cut septum). Prior to every cut made, the two exposed ends of the tissue were glued with paper backing and a small piece of suture was attached to the posterior-apex part of the septum in order to keep track of the orientation of the septum while slicing. Next, the tissue was placed inside the slicing groove and was held in a rigid fashion using the suture ends. The blade was then brought down swiftly on the septum and the tissue was cut into two slices. This first cut was at half the initial thickness of the septum. Once cut, face three was revealed. The α measurements were taken off face three and recorded. The paper and suture were then attached to both surfaces of face three and each slice was halved again revealing faces two and four. α was measured and recorded from these faces as well. The α measurements of each face were averaged to give an α value for every face. Next, the mean α measurement for TQ1 was found by taking the average of α values of face 1 and face 2. Similarly α values for other quarters were found. The α value of face 5 was not measured due to fiber disarray. Hence a linear equation was fit using the data from the other faces in order to estimate an α value for face 5.
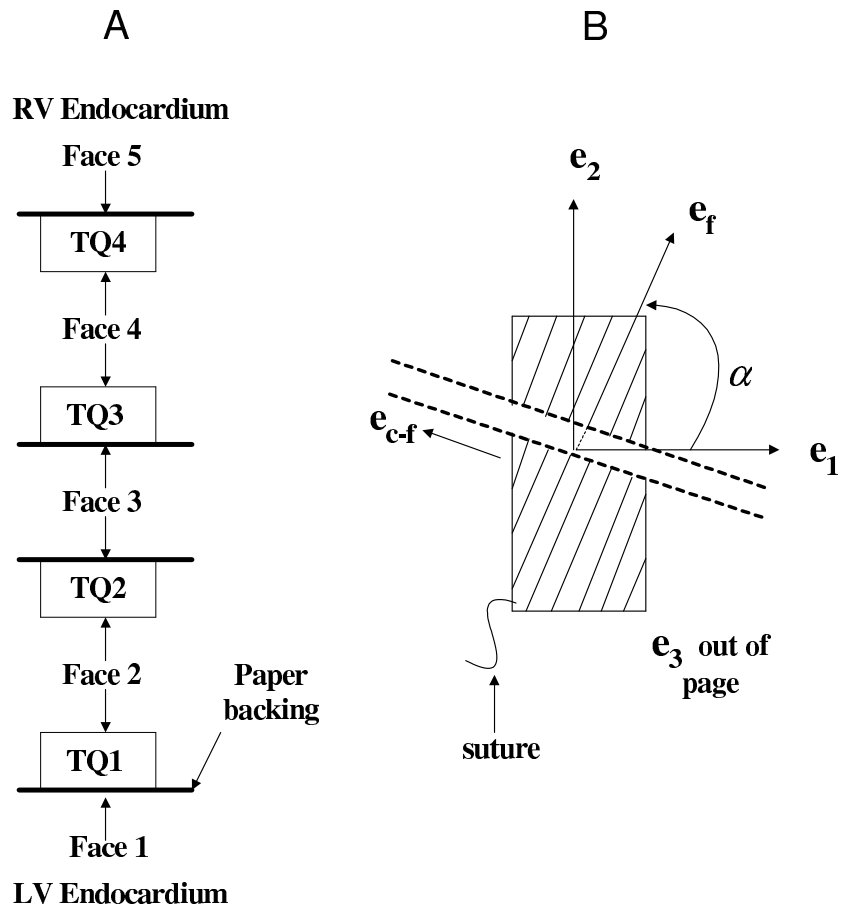
Fig. 9. Fiber Angle Measurement; Note: A. Cross-section of cut septum showing faces and depths B. Fiber angle measurement for TQ1: face 1 glued down, viewing face 2

A. TQ1: Face 1 glued down, viewing face 2

e_2

$+e_f$

$+e_{c-f}$

e_1

e_3 out of page

suture

B. TQ2: Face 3 glued down, viewing face 2

e_2

$+e_f$

$+e_{c-f}$

e_1

e_3 into page

suture

C. TQ3: Face 3 glued down, viewing face 4

e_2

$+e_{c-f}$

$+e_f$

e_1

e_3 out of page

suture

D. TQ4: Face 5 glued down, viewing face 4

$+e_{c-f}$

e_2

e_1

$+e_f$

e_3 into page

suture
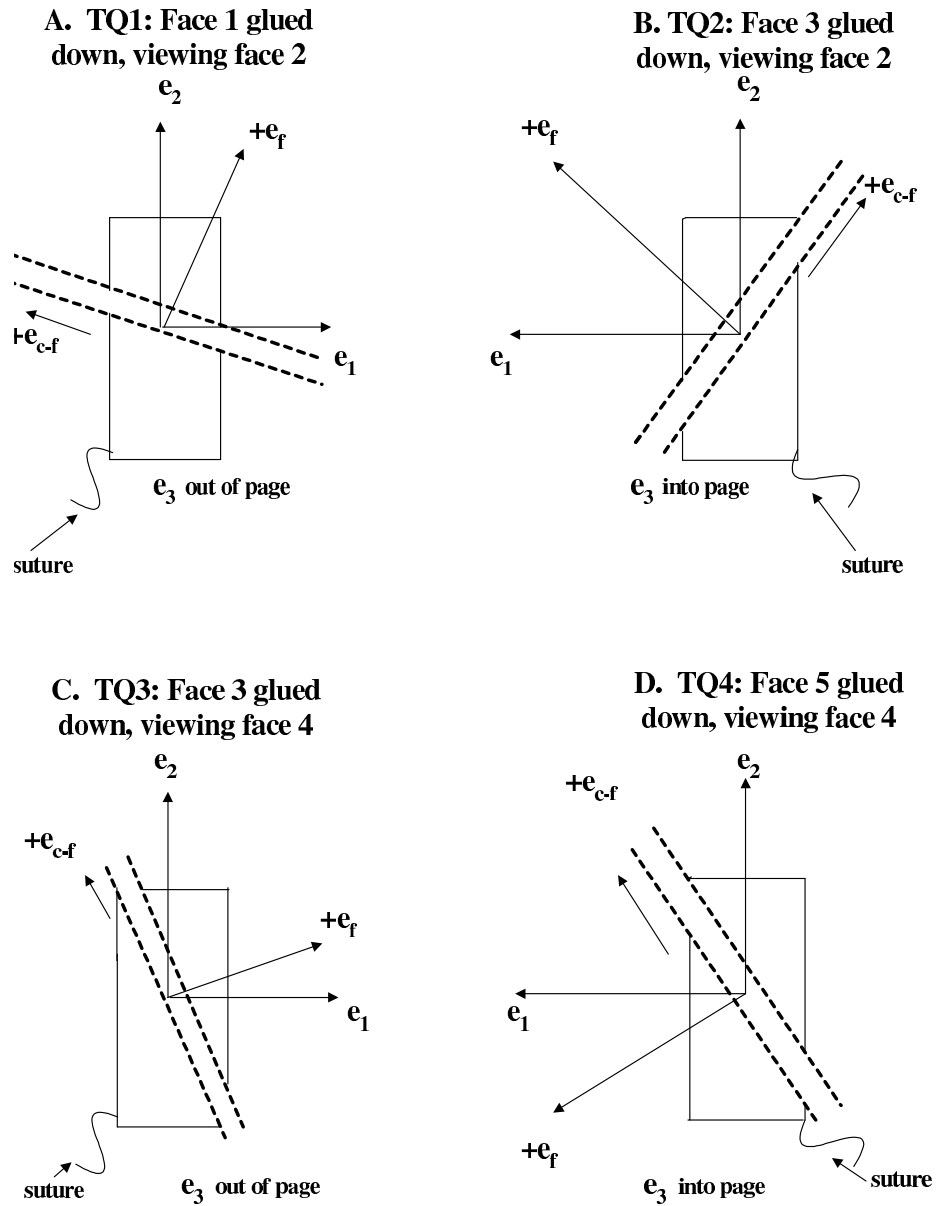
Fig. 10. Templates for Cross-fiber Measurement; Note: A. TQ1: Face 1 glued down, viewing face 2; B. TQ2: Face 3 glued down, viewing face 2; C. TQ3: Face 3 glued down, viewing face 4; D. TQ4: Face 5 glued down, viewing face 4

1. Sheet Angle Measurement

Sheet Angle "β" is the angle subtended by the sheet axis e_s to the positive radial direction e_3.

The four sections representing the transmural quarters of the septum, resulting from the cuts done for measurement of fiber angle, were then placed in an infiltrating solution for one week (JB4 embedding solution) (Polysciences Inc, Warrington, PA) until the tissue appeared translucent and sank to the bottom of the test tube. Templates with e_1, e_2 and e_3 drawn were prepared for every quarter. Once the tissue slices were properly infiltrated, they were glued paper side down on the templates and the fiber axis e_f was marked. The cross-fiber direction e_{c-f} ($\alpha + 90°$) was located and the quarters were cut with a blade along e_{c-f} in the upper one-third of the tissue to reveal two slices for every quarter as shown in Figure 10. These slices were then rotated by 90° such that we got a cross-fiber view of the slice with the fiber axis e_f pointing out of the page. With this arrangement, as shown in Figure 11 the sheet axis e_s was in the plane of observation which would later allow direct measurement of the sheet angles. The cut slices were placed in molds filled with hardening solution (JB4 hardener, epoxy resin)(Polysciences Inc, Warrington, PA) put in airtight containers (we used sealable plastic bags) and placed in the refrigerator for a week until they were appropriately hardened. Following this, they were removed from the molds and sliced to 10 μm using a microtome. Digital images of these slices were obtained and the sheet angles were measured. In order to avoid the distorting effects of paraffin embedding we chose to use aqueous embedding which reduced the dehydration of the tissue blocks. Nevertheless, there was some dehydration as evidenced by gaps between the myolaminae. In fresh heart tissue there are no voids or gaps. As addressed in the legend of Figure 11, gaps were not due to the slicing process, but due to dehydration

or residual stress present in the tissue. This is so because the gaps are filled with epoxy embedding media whereby they had to be present in the tissue block prior to slicing.
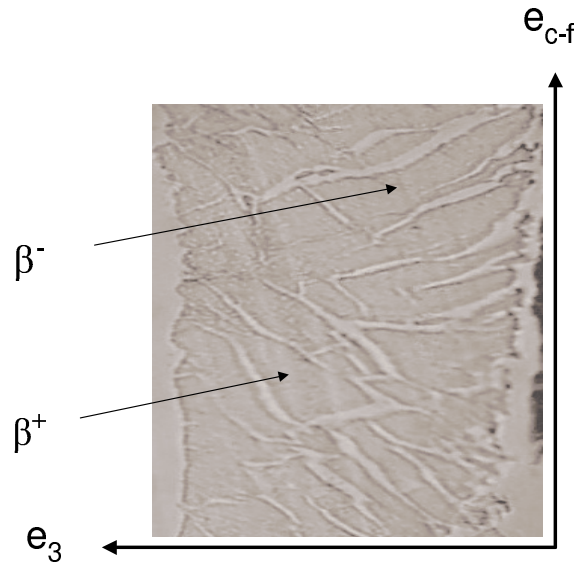
Fig. 11. Cross-fiber View of Sheets at TQ2; Note: Right handed local co-ordinate system formed by (e_f, e_{c-f}, e_3) representing the fiber axis (going out of the plane of paper), cross-fiber axis and radial axis respectively; Seen in this block of tissue are two different sheet families represented by β^+ and β^- corresponding to positive and negative sheet angles respectively. It is important to note that the gaps between sheets are not an artifact of slicing. There is epoxy embedding media filling the space between the sheets, and slices were intact when mounted (continuous knife marks can be seen in the image)

While imaging the sheets, the positive cross-fiber direction was always maintained at the top of the image as shown in Figure 11. In order to obtain the angle, data points were collected from around the edge of each sheet in the image. These points were then put into a Matlab program that filled in the remainder of points to make a complete set of pixels to represent the sheet cross-section (to be more specific, the

cross-fiber cross-section of the sheet). Since the sheets were more rectangular than elliptical, we computed an effective major axis vector which was the sheet axis e_s. Once the vector was obtained, the sheet angle was calculated as

$$\beta = -tan^{-1}(\frac{y}{x}) \tag{3.1}$$

where "x" and "y" represent the x and y co-ordinates of the major-axis vector e_s. Positive e_3 represented $\beta = 0°$. β was positive when the rotation from e_3 to e_s was clockwise and negative when counter-clockwise. The negative sign is in accordance with our sign convention. A histogram of the sheet angle measurements revealed multiple sheet families. The family with the largest number of measurements was then averaged and identified as the dominant sheet angle for that particular quarter. Sheet angles were calculated in the above manner for all septae of both groups of data.

2. Thickness, Total Number of Sheets

The thickness of the sheets at every depth was measured using a MATLAB program. The thickness of the sheets was measured in mm. Total number of sheets present at every depth of the septum was also counted.

3. Uniformity Index

In order to quantify the transmural dispersion in sheet angle values, we defined a uniformity index. Total number of positive and negative sheet angles was measured at each quarter of the septum. Uniformity Index was defined as:

$$UI = \frac{P - N}{P + N} \tag{3.2}$$

Table I. Uniformity Index Interpretation

UI Values	UI = 1	UI = -1	UI = 0	UI > 0	UI < 0
	N = 0	P = 0	P = N	P > N	P < N
What they mean	Sheet angles uniformly positive	Sheet angles uniformly negative	No uniformity	Mostly positive sheet angles	Mostly negative sheet angles

where P and N represent number of positive and negative sheet angles respectively. Table I summarizes what different values for the UI mean in terms of sheet angle uniformity and how we will interpret the results based on these values.

4.   Statistical Tests

One-tailed or two-tailed unpaired t-tests were performed on the data sets. If the p-value was $p < 0.05$, then the HS data was considered to be significantly different from the data obtained from the controls group (LS data). In all the figures and tables below, * is used in order to indicate statistical significance.

CHAPTER IV

RESULTS

A. Evidence of Hypertrophy of HS Rats

To confirm evidence of hypertrophy in the HS rats, we compared the heart weight to body weight ratios and the thickness of the septum-to-outer-radius ratios of both the groups of data. The following results provided evidence of hypertrophy in the HS group of rats.

1. Heart Weight to Body Weight Ratio

The HS rats had a higher mean HW/BW ratio (0.005 ± 0.0003) as compared to the LS group of rats(0.0032 ± 0.0002) as seen in Figure 12. That is a 58% increase in HW to BW ratio similar to (32). This is due to the significant decrease in the body weights of the HS groups of rats that were fed the HS diet.
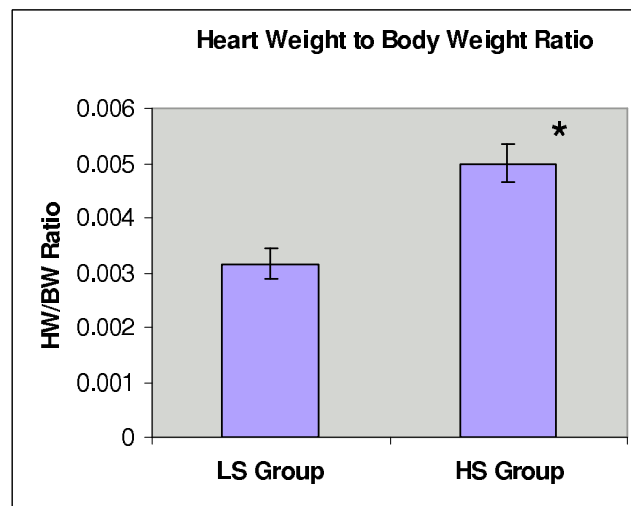
Fig. 12. Heart Weight to Body Weight Ratio; Note: * indicates statistical significance: $p < 0.05$

2.   Thickness to Outer Radius Ratio (T-R ratio)

The HS rats had a slightly higher mean thickness to anterior-posterior outer radius ratio (0.569 ± 0.082) than the LS rats (0.560 ± 0.067) as seen in Figure 13. The HS rats also had a slightly higher mean thickness to left-right outer radius ratio (0.642 ± 0.146) than the LS group (0.6 ± 0.0693), yet the differences in both cases were not significant.
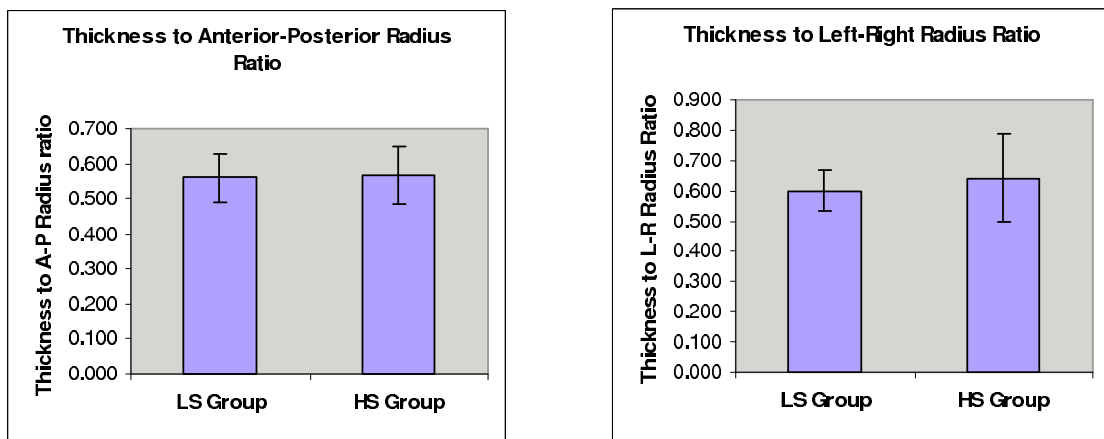
Fig. 13. Thickness to Outer Radius Ratio

3.   Heart Weights

The heart weights of both the groups were not significantly different as seen in Figure 14A. (LS: 1.30g ± 0.113, HS: 1.265g ± 0.166)

4.   Body Weights

Figure 14B shows that the body weights of the HS group decreased significantly (254.167g ± 23.752) as compared with the LS group (418g ± 26.055), due to the deteriorating condition of the HS hearts as a result of being fed the HS diet.

5. Thickness of the Septum

Figure 14C reveals a comparison of the thickness of the septae of the two groups. There is a slight decrease in the septum thickness of the HS group (3.141mm ± 0.332) as compared to the LS group (3.2mm ± 0.479), though the difference is not statistically significant.
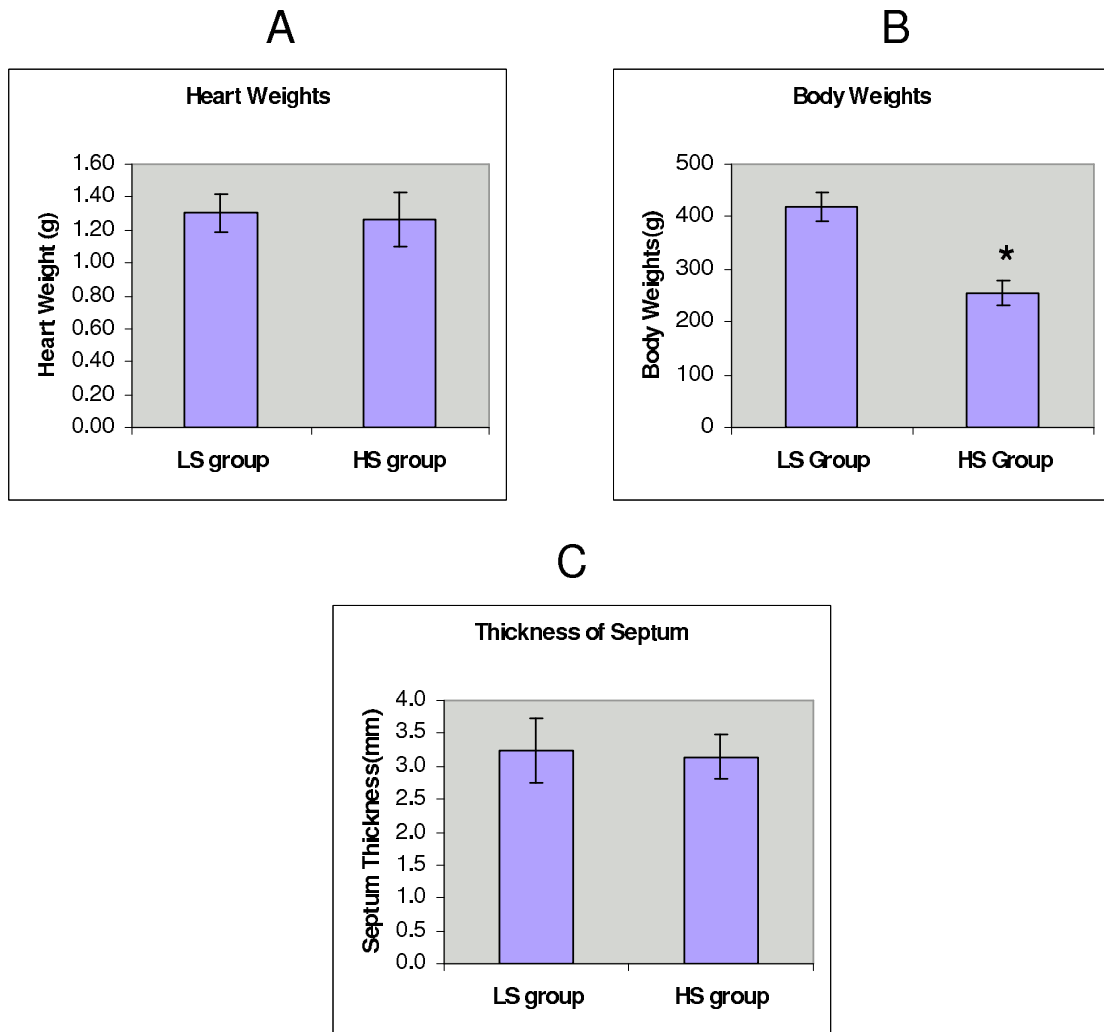
Fig. 14. Individual Measurements; Note: A. Heart Weights B. Body Weights C. Thickness of Septum; * indicates statistical significance: p < 0.05

6. Transitional Eutrophy

An observation of the results above shows that both the groups of rats had almost similar thickness to radius ratios and heart weights. This meant that although the shape and size of the HS group of hearts look like the LS groups of hearts, they have undergone a totally different mechanical history as they are in transition from the concentric hypertrophy phase (charaterized by increased thickness to radius ratios) to the dilated hypertrophy phase before heart failure (characterized by reduced thickness to radius ratios and chamber dilation). Concentric hypertrophy as well as dilated hypertrophy are well-documented states in previous studies (32). Yet, a stage of hypertrophy that lies in between these two states has never been captured before to our knowledge. A comparison of the two groups of data in the light of this discovery makes our study significant.

"***Transitional Eutrophy***" (derived from the Greek work "*eutrophos*" meaning well-nourished; in our context used to mean normal state) is a term that we have coined to define the heart stage with normal size and shape but in transition from pressure-overload (concentric) hypertrophy to dilated hypertrophy. Figure 15 illustrates the stage of hypertrophy of the heart represented by transitional eutrophy during the progression to heart failure.

B. Fiber and Sheet Morphology

1. Total Number of Sheets

Figure 16 shows the total number of sheets measured at all four depths of the septum. At every depth of the septum, it is seen that total number of sheets in the HS group of rats increased significantly as compared to the LS group of rats. Table II summarizes total number of sheets as measured in both groups. Increase in total number of sheets

**STAGES OF HYPERTROPHY DUE TO SUSTAINED
PRESSURE OVERLOAD--THE PATH TO HEART FAILURE**
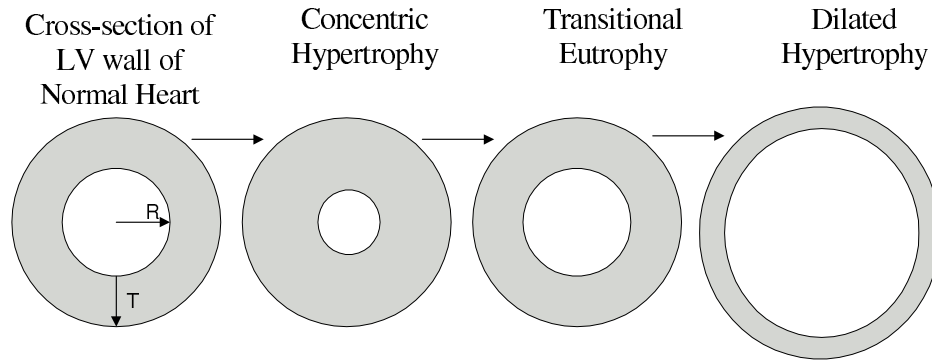
T = Thickness; R = Radius

Fig. 15. Transitional Eutrophy

of the HS group is: TQ1 = 176%, TQ2 = 356%, TQ3 = 290%, TQ4 = 207%. Overall, the number of sheets approximately tripled (200% increase).

2.   Thickness of Sheets

Figure 17 shows the thickness of the sheets measured at all four depths in both the groups of data. The thickness of the sheets has been reported in mm. In all four cases it is evident that the thickness of the sheets decreased significantly in the HS group as compared with the LS group. Decrease in mean sheet thickness of HS group: TQ1 = 42%, TQ2 = 38%, TQ3 = 29%, TQ4 = 34%. Table III summarizes the sheet thickness in both groups.
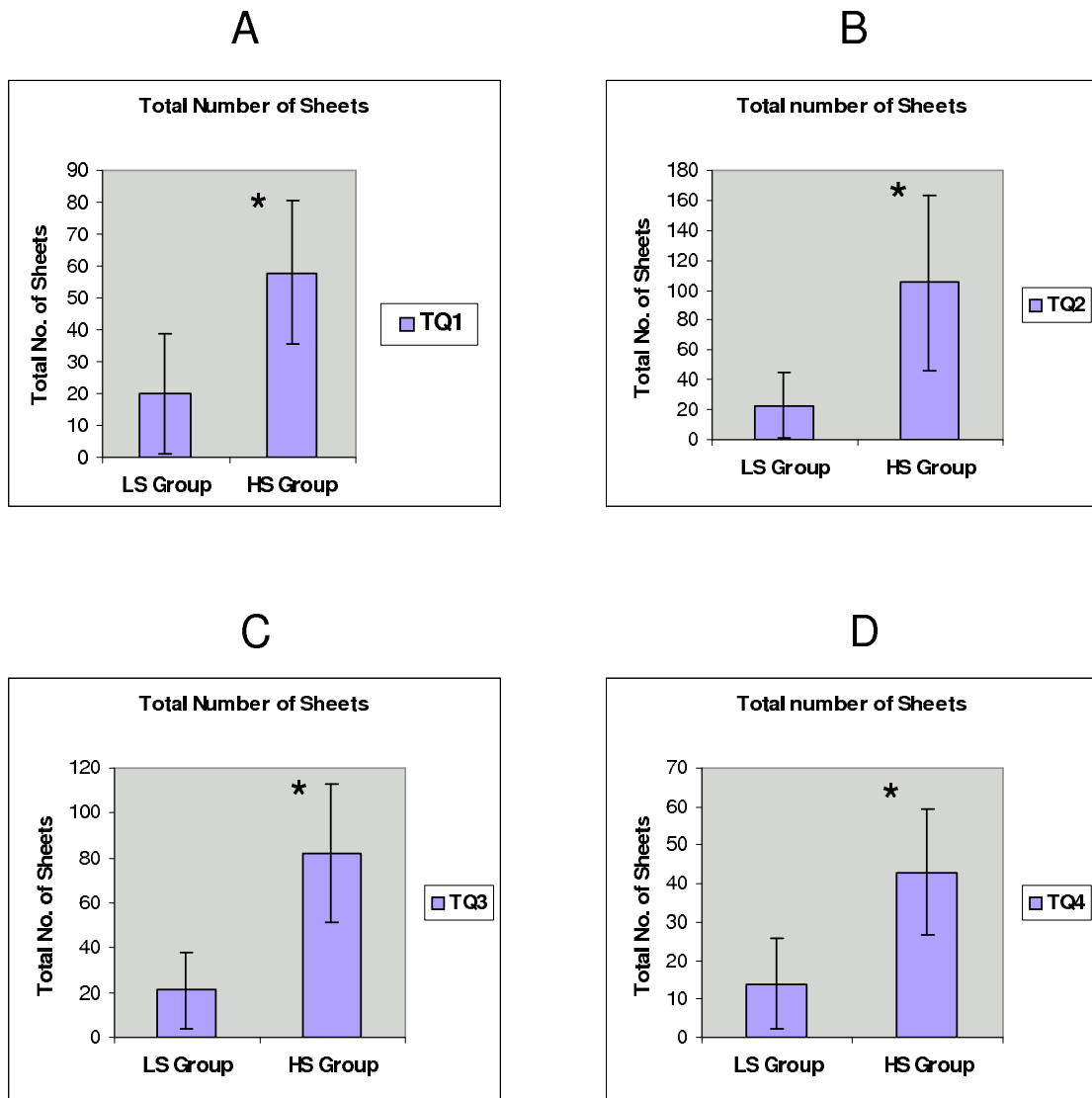
Fig. 16. Total Number of Sheets; Note: A. TQ1 B. TQ2 C. TQ3 D. TQ4; * indicates
statistical significance: $p < 0.05$

Table II. Total Number of Sheets; Mean $\pm$ 1 Standard Deviation; * indicates statistical significance: $p < 0.05$

Transmural Quarter	LS Group	HS Group
TQ1	20 $\pm$ 19.733	58 $\pm$ 22.586*
TQ2	23 $\pm$ 21.561	105 $\pm$ 58.329*
TQ3	21 $\pm$ 16.736	82 $\pm$ 30.901*
TQ4	14 $\pm$ 11.705	43 $\pm$ 16.3*

Table III. Sheet Thickness (mm); Mean $\pm$ 1 Standard Deviation; * indicates statistical significance: $p < 0.05$

Transmural Quarter	LS Group	HS Group
TQ1	0.143 $\pm$ 0.085	0.0829 $\pm$ 0.0167*
TQ2	0.148 $\pm$ 0.039	0.091 $\pm$ 0.0139*
TQ3	0.137 $\pm$ 0.023	0.0974 $\pm$ 0.0185*
TQ4	0.181 $\pm$ 0.070	0.1191 $\pm$ 0.0304*
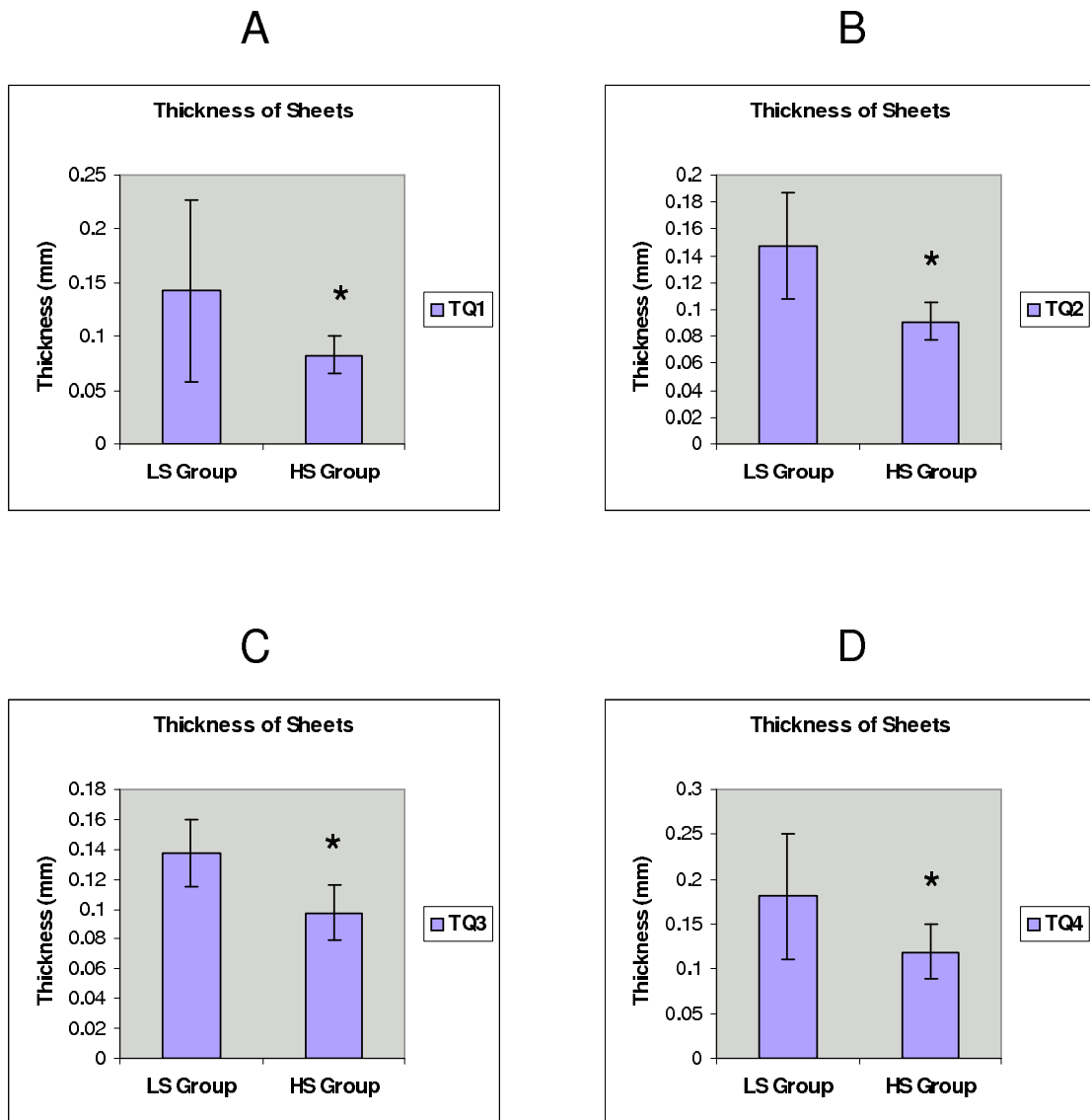
Fig. 17. Sheet Thickness; Note: A. TQ1 B. TQ2 C. TQ3 D. TQ4; * indicates statistical
significance: $p < 0.05$

Table IV. Fiber Angles(degrees) Mean ± 1 Standard Deviation; * indicates statistical significance: p < 0.05

Transmural Quarter	LS Group	HS Group
TQ1	62.486° ± 12.566°	95.7° ± 13.916°*
TQ2	29.898° ± 13.755°	50.948° ± 20.782°*
TQ3	-7.261° ± 13.482°	-14.818° ± 20.598°
TQ4	-44.201° ± 16.078°	-12.2214° ± 21.8022°*

3. Fiber Angles

As seen in Figure 18, in the LS group the mean fiber angles varied from $62° ± 12°$ at TQ1 to $-44° ± 16°$ at TQ4. The HS group showed a statistically significant increase in fiber angle values at the measured depths of the septum (except at TQ3) ranging from $96° ± 14°$ at TQ1 to $-12° ± 22°$ at TQ4. Note that the total span in fiber angle from inner to outer is the same in LS and HS groups ($108°$). Increase in mean fiber angle was as follows: TQ1: 53%, TQ2: 70%, and TQ4: 72%. Table IV below summarizes the fiber angle results.

4. Sheet Angles

Table V summarizes the sheet angles measured at all four depths of the septum. Sheet angles were not statistically significant as seen in Figure 19.

5. Uniformity Index

As summarized in Table VI, the uniformity index was not statistically significant in HS group but showed an alternating change of sign while transitioning from TQ1 to TQ4.
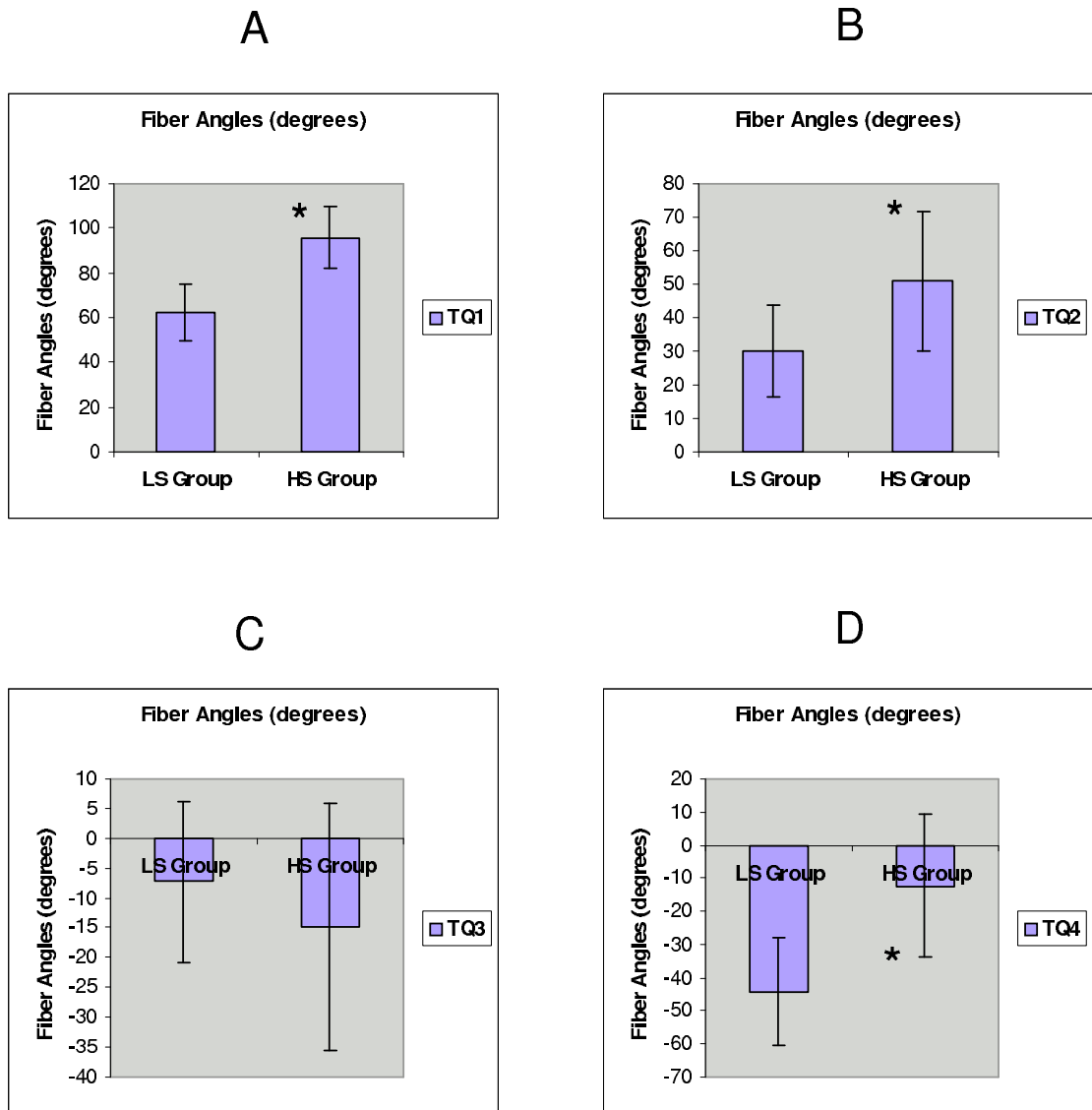
Fig. 18. Fiber Angles; Note: A. TQ1 B. TQ2 C. TQ3 D. TQ4; * indicates statistical significance: p < 0.05
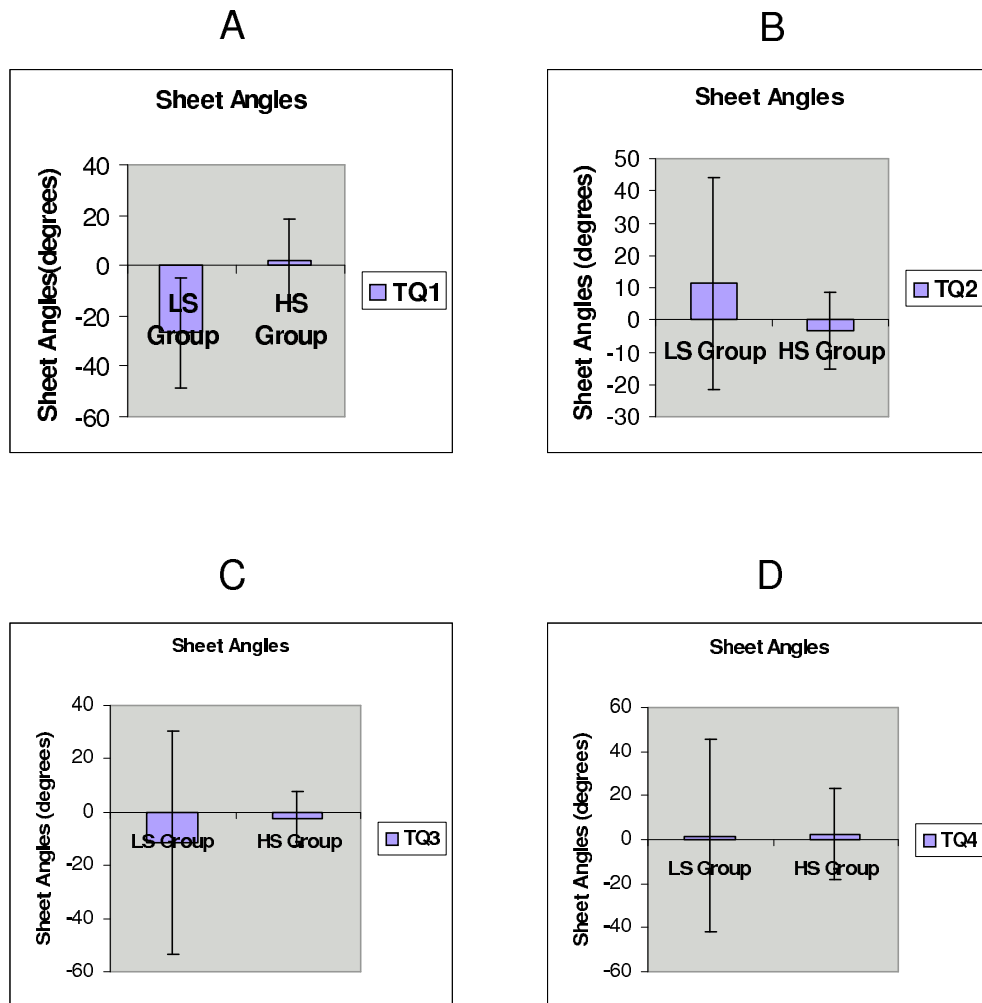
Fig. 19. Sheet Angles; Note: A. TQ1 B. TQ2 C. TQ3 D. TQ4

Table V. Sheet Angles; Mean ± 1 Standard Deviation

Transmural Quarter	LS Group	HS Group
TQ1	-26.526° ± 21.86°	1.929° ± 16.305°
TQ2	11.359° ± 32.733°	-3.34963° ± 11.775°
TQ3	-11.4435° ± 41.801°	-2.635° ± 10.294°
TQ4	1.684° ± 43.919°	2.461° ± 20.386°

Table VI. Uniformity Index; Mean ± 1 Standard Deviation

Transmural Quarter	LS Group	HS Group
TQ1	-0.287 ± 0.548	-0.102 ± 0.67
TQ2	0.277 ± 0.666	-0.1462 ± 0.465
TQ3	-0.163 ± 0.663	-0.154 ± 0.284
TQ4	0.344 ± 0.5611	-0.164 ± 0.2

C.   Discussion of Results

The principal finding of this study is the significant increase in the total number of sheets along with a significant decrease in the mean sheet thickness at all four depths of the septum in hearts that are at the stage of transitional eutrophy-a heart stage with normal size and shape yet in transition from concentric hypertrophy to dilated hypertrophy. Previous studies (32) have shown that hearts moving from the concentric to dilated hypertrophy stages transition from having an increased thickness to radius ratio (hallmark of concentric hypertrophy) to a decreased thickness to radius ratio (dilated hypertrophy). Hence, a stage that lies almost equally between these two states would be characterized by hearts that have a thickness to radius ratio resembling the control group (LS group) of hearts. Because myocyte shape is thought to map directly to ventricular shape, it was expected that hearts of the same shape and size would share similar fiber and sheet structure. It was anticipated that the thickness of sheets, fiber angles and number of sheets of both the groups would be similar. Hence an unexpected finding of this study was the significant increase in the number of myolaminae (sheets) which themselves were significantly thinner than the control group.

While there are several reports in the literature regarding changes in the shape, size and number of myocytes with remodeling (22, 5, 24, 3), there is very little documentation regarding the same of myolaminae. Most studies focus on the previously defined states of hypertrophy viz. concentric and dilated hypertrophy, hence comparative studies of the microstructure for this phase of heart failure are complicated by shape change. Anversa et al. (5) showed that in the left ventricular myocardium of rat heart after 14 weeks of hypertension, the number of myocytes remained constant although there was an increase in the size of myocytes with hypertrophy. The

number of myocytes per sheet were not measured, yet it would need to be declining with hypertrophy if the cell diameter increases while the sheet thickness decreases. Future studies to investigate this would be needed. Such a dramatic change in sheet thickness and number was not expected. Thus the current study was not designed to measure the number of cells per sheet in the thickness dimension.

In both the LS group and HS group, the largest mean thickness of sheets was observed at TQ4 (wall closest to the epicardium). In the low-salt diet group, lowest mean thickness was observed at TQ3 while in the high salt group, lowest mean thickness was observed at TQ1. The mean total number of sheets measured at all four transmural depths of the septum increased significantly in the HS group as compared to the LS group. TQ2 had the largest number of sheets while the TQ4 had the fewest number of sheets in both groups of data.

Since more sheets translate as more myocytes, this result is in agreement with Anversa et al. (5) who found that in normal rat hearts endocardial regions had 30% more myocytes compared to the epicardial regions. It has been previously shown that interlaminar shear and overall maximum shear strain are greater in magnitude at the endocardium than the epicardium (18). This could mean that a larger number of sheets would be needed in and around the endocardium and fewer at the epicardium. Our data supports the observation that the wall closest to the epicardium (TQ4) experiences the lowest shear deformation due to least number of sheets present which are also the thickest sheets in both groups of data.

In the LS group, fiber angles varied from approximately +60° at TQ1 (wall closest to LV endocardium) to -44° at TQ4 (wall closest to RV endocardium); fiber angles in the HS group ranged from 96° at TQ1 to -12°. In normal hearts of various species, studies have reported a transmurally varying myofiber orientation varying from around -60° at epicardium to +60° at endocardium (29, 23, 63). As the

heart progresses from compensated hypertrophy stage into the decompensated state towards failure, wall thickness reduces and walls start thinning due to side-to-side slippage of myocytes (1). In addition to this reason, the clear increase in the values of the fiber angles in the HS group could be as a result of fiber re-arrangement due to myocyte/sheet loss along with simultaneous elongation of existing myocytes. Further studies would need to be done to investigate this theory. Since the total span in fiber angle was constant ($108°$) for LS and HS groups, it must be emphasized that the tissue block was excised with cuts parallel to the long axis of the heart and that the hearts were fixed at the same filling pressure (1 kPa). However, if there is a different volume vs. twist relation for the hypertrophied heart versus the normal heart, then there could be an overall shift in fiber angle span with no shift of the quarter nearest zero. This is the pattern that was measured, and hence it can be explained by different amounts of passive stiffness and perhaps residual stress in the hypertrophied heart. To differentiate twisting type motion from actual fiber direction change, more information is needed on the wall mechanics. The fixation pressure was chosen to be that of end-diastole (10cm H_2O), and in our opinion, a comparison at this passive state is more physiological than one at a zero pressure state.

Sheet angles varied from approximately -27° at TQ1 to around 0° at TQ4 in the LS group and were approximately around 0° in the HS group. This is probably due to the large number of sheets with several sheet families present which made identification of the dominant sheet family unclear. Since there was quite a large standard deviation in the sheet angle data, we defined the uniformity index in order to account for the dispersion in the values of the sheet angles. How to best quantify sheet orientation and structure is still an open question in our opinion. For lack of a better metric, we chose to report the mean angle of the largest sheet family and a uniformity index to characterize how uniform the entire population of one quarter is.

Advancement in sheet structure morphometrics is needed.

In the low-salt diet group, at TQ1 the sheets were more negatively oriented, at TQ2, the sheets were more positively oriented, at TQ3, they were again positively oriented and at TQ4, they were negatively oriented. This is in agreement with the accordion-like laminar structure described by Harrington et al. (29) that could contribute to systolic wall thickening mechanism in the normal hearts.

Sheet extension, thinning and shear appear to contribute significantly to systolic wall thickening (18), (64). However, in the high salt group, we noted that at all four septum depths, the sheets were negatively oriented. This means that the transmural laminar variations reduce as the hearts hypertrophy and progress towards failure. Since the epicardium undergoes much less shear deformation relative to the endocardium (18), it stands to reason that the transmural laminar variations are directly modulated by the shearing deformation of the sheets. An end-stage heart failure model would be a good group of rats to study next to test this hypothesis of shear mediated sheet remodeling because previous studies (32) have shown that as the hearts progress into the dilated hypertrophy stage before heart failure the thickness to radius ratio decreases whereby the transmural variations in shear deformation are subsequently reduced.

Fiber orientation which varies in most species from approximately -60° at the epicardium to +60° at the endocardium (29, 23, 63) can be measured directly. Sheet angles though, traditionally have not been viewed directly. Indirect methods infer the sheet directions using fiber directions and cleavage planes from three orthogonal views (18), and rely on an assumption that sheet morphology is uniform within the block with faces determined by the three orthogonal views. Confocal microscopy has been used (71) to provide quantitative structural information about the 3D organization of myocytes and extracellular collagen matrix; however such methods are not

yet optimized for high throughput as needed to compare two groups with moderate numbers (10 per group). Our quantitative histology method for sheet and fiber structure permits high throughput and has been used successfully for direct sheet angle measurement in sheep and canine hearts (10, 29). It ensures that the fiber and sheet structure remain intact and can be used for sheet angle measurement for any mammalian species that is the size of rats or larger.

CHAPTER V

GROWTH MODEL

A.   Significance of the Model

Numerous investigations of the myocardium have focussed on the study of the individual myocyte. However, the myocardium is an integrated structure with the fundamental unit of the microstructure being the myolamina-a sheet of myocytes that is three to four cells thick, surrounded by collagen. An understanding of how the myolamina responds to a change in its mechanical environment is vital as it will help towards better disease diagnosis as well as help build medical devices more suited to the specific problem at hand. The present study is a unique one as it has captured the morphology of the myolaminae (sheets) in a state of transition from pressure-overload hypertrophy to dilated hypertrophy. The results of this study have prompted us to present the details of what actually happens at the level of the myolaminae as the myocardium progresses toward failure. This model will present a clear picture of sheet morphology at every stage of hypertrophy. This knowledge will help further our understanding of the role sheet mechanics in the diseased myocardium. Knowledge of the sheet behavior will also foster research geared to determine innovative treatment methodologies for people suffering from CHF.

B.   Background on Individual Myocyte Behavior during Overload

1.   Pressure-Overload Culminating in Heart Failure

Concentric hypertrophy or pressure-overload hypertrophy, although considered to be a protective and adaptive response to pressure-overload states as seen in arterial hypertension or LV outflow tract obstruction, may cause reduction in chamber dis-

tensibility accompanied by increased chamber stiffness. According to Peterson (50), with sustained pressure overload, the increased afterload imposed by the hypertension or the LV outflow obstruction, following observations have been noted in various experimental and clinical studies (not necessarily in the order stated):

- An imbalance is struck between muscular (myocytes) and nonmuscular components (fibroblasts, endothelium, mitochondria) of myocardium resulting in tissue heterogeneity.

- Fibrosis is observed in the interstitium and preivascular areas and scarring replaces necrotic myocytes.

- The increased afterload imposed by hypertension or LV outflow obstruction outstrips the adaptive mechanisms.

- The LV dilates, myocardial contractility may be normal or diminished (57, 58, 59, 17, 32), diastolic chamber stiffness is normal or decreased (43, 51, 30) and myocardial stiffness is normal or increased (43, 51, 30).

- Preload reserve becomes exhausted despite LV chamber dilation resulting in reduced speed of shortening of LV chamber leading to inadequate cardiac output (55).

- Simultaneous elevation of both LV end-diastolic pressure and left atrial mean pressure gives rise to pulmonary congestion. Thus, the clinical symptoms of CHF are manifested in a person suffering from chronic pressure overload.

Several studies have dealt with the changes that take place at the myocyte level during the hypertrophy states (pressure and volume overload) as the heart transitions towards failure. Yet, such studies at the myolaminae/sheet level are relatively few.

It would be worthwhile to take a look at studies that have looked into changes in myocyte morphology of the heart in overload conditions. This will help shed some light on the probable behavior of myolaminae under similar conditions.

2. Myocyte Proliferation in the Overloaded Heart

For the last fifty years, it has been widely accepted that the the heart responds to an increase in workload by hypertrophy of existing myocytes. When this myocardial hypertrophy is exhausted, the cells die and heart failure is manifested. The difficulty in identifying mitotic figures in tissue sections originated the concept that myocytes cannot divide. Yet there have been numerous findings that suggest the ability of the mammalian heart to replicate and respond to pathologic loads by myocyte proliferation (2). Linzbach (40) was one of the first few researchers to propose that cardiac hypertrophy in humans was a result of myocyte hyperplasia and myocyte hypertrophy. He showed that when a critical weight of 500g or greater is reached in the human heart cell regeneration begins. In the past decade, the availability of the confocal microscope allowed visualization and quantification of mitosis in tissue sections (6, 4, 33). Linzbach's theory was also confirmed by several more recent studies (3, 56, 25) .

Studies in animals and humans have shown that the degree of overload is an important factor in the initiation of myocyte hypertrophy and hyperplasia. Thus, when there is a gradual or a moderate increase in workload (45), myocyte hypertrophy dominates; a severe increase in workload (acute/chronic), may result in mitosis resulting in myocyte proliferation (33, 11, 46). Olivetti et al. (48) showed that long-term pressure overload in the right ventricle resulted in a 44% increase in the number of myocytes along with a 24% increase in myocyte diameter and a 22% increase in intermyocyte distance. These increases helped to decrease the magnitude of the sys-

tolic and diastolic stresses on a per cell basis thus improving the myocardial response. Also, it has been observed that myocyte hyperplasia is accompanied by little or no hypertrophy in diseased hearts of both humans (54) and animals (16). It has been shown that prolonged systemic hypertension in rats results in cellular hyperplasia inspite of diffuse tissue injury (47, 8). Hence, it seems that myocyte proliferation characterizes the phase of transition from compensated hypertrophy to cardiac dysfunction. Yet the transition from enlarged myocyte(at the compensated stage) to nuclear proliferation is unclear.

The impact of duration of the disease is an important one and needs several groups of hearts to be studied at distinct time points to understand the changes that evolve during the process (4). Increases in the number of myocytes in the overloaded rat heart vary from 20% to 45% (3). Since the progression of the disease involves myocyte loss by necrosis and apoptosis (both are processes that lead to cell death), cell death and cell growth occur simultaneously (4). Hence the myocyte loss results in an underestimation of myocyte proliferation whereas the myocyte proliferation leads to an underestimation of myocyte death. Thus the myocyte cell numbers may not provide an accurate picture of cell regeneration whereas myocyte loss obscures myocyte proliferation. It has been found that in terminal failure, cell death exceeds cell proliferation (33, 11, 28); yet without knowledge of duration of apoptosis and necrosis, interpretation of these results is questionable .

3. Myocyte Loss in the Overloaded Heart

According to Levy et al.(38) hypertension affects the myocardium in two stages:

- **Stage 1**: Pressure-overload is characterized by a period of compensation during which the contractile function is preserved and systolic wall stress is normal.

- **Stage 2**: This well-compensated period which varies from weeks (in rodents) to months and even years (in humans), is inevitably followed by a transition to failure. This transition phase is characterized by chamber dilatation and progressive contractile dysfunction due to the inability of the hypertrophic growth to normalize the load. This phase is also marked by a significant loss of myocytes by both apoptosis and necrosis (7) along with changes in the cytoskeleton of the myocytes (66) and alterations of the extracellular matrix (68).

Apoptosis is a physiologic mechanism of cell deletion for maintenance of tissue integrity. It is called programmed cell death because it is genetically regulated. Unlike necrosis, cells undergoing apoptosis show no signs of swelling or membrane rupture. Apoptotic cells shrink and maintain their membrane integrity. Recently it has been shown that myocyte apoptosis and proliferation are simultaneously present in several situations (7). Increased apoptosis was noticed in the left ventricle of spontaneously hypertensive rats (SHRs) compared with the normotensive control rats in a study by Li et al. (39). It was demonstrated in this study that there is an increase in myocyte apoptosis in hearts from failing rats compared with nonfailing SHRs. Thus it is possible that apoptosis may be the mechanism by which myocyte loss occurs in the transition from stable compensated hypertrophy to heart failure. Also, in the terminal stages of failure, cell death is thought to take place by apoptosis which is an ongoing process distinctly different from myocyte necrosis and tissue fibrosis. Some of the factors potentially involved in the apoptosis of myocytes in hypertension are: mechanical overload, ischemia, angiotensin II, calcium overload and mitochondrial defects (20). Does apoptosis account for the exaggerated loss of myocyte described in humans with hypertension? This is still an open question for future research.

Necrosis is unprogrammed cell death. Unlike apoptosis, it is nonregulated and a nonphysiologic form of cell death (20). This disorderly cell death does not send signals to the nearby phagocytes (cells that ingest or destroy foreign matter/debris through a process called phagocytosis) to clean up the cell debris. This lack of signaling causes inability of immune system to recycle the dead cells which results in swelling of the cells and rupture of the cell membranes (65). These injuries received by the cells may release enzymes and harmful chemicals that could damage other cells.

Accumulation of fibrous tissue is an important feature of structural remodeling of the myocardium during hypertensive disease. This fibrosis is neither a result of myocyte growth nor necrosis. It represents a reactive process (69). The fibrous tissue formation occurs as a result of population of fibroblasts that regulate their turnover of collagen in an auto-paracrine manner. Fibrous tissue is mainly composed of type I collagen and to a lesser extent type II collagen. In hypertensive heart disease, morphologically, it represents a reactive perivascular fibrosis of coronary arteries and arterioles with extensions into the interstitium to create interstitial fibrosis (70). Microscopic scarring which is a reparative fibrosis replaces myocytes lost due to necrosis (69).

Thus, structural remodeling of the myocardium due to pressure-overload involves an amalgamation of all the above types of cell death as well as cell regeneration caused by proliferating myocytes.

C.   Proposed Growth Model

The proposed model depicts in a pictorial fashion the various phases of hypertrophy as the heart transitions toward failure on being subjected to the sustained pressure overload. In the present study our animal model was male Dahl-salt sensitive rats

that were subjected to pressure overload by being fed a high-salt diet from the age of 6 weeks until 11-13 weeks after which they developed pulmonary congestion and were sacrificed. The proposed model seeks to explain the changes that may occur in the myocardium at the sheet level as it is subjected to excessive pressure overload. The predictions of this model are based on the results of this study as well as past research on the changes that the myocyte undergoes as the heart progresses toward failure. The behavior of the sheet is directly influenced by the behavior of the individual myocytes. Hence, the theory of this model is dictated in part by the individual myocyte behavior at the different stages of hypertrophy before failure.

Figure 20 represents the proposed model. The model presents a pictorial representation of sheet structure at the various stages of hypertrophy leading to failure. A single myolamina cross-section is represented as a rectangle and is 3-4 myocytes thick in diameter (shown as circles inside the sheets in Figure 20). Note that the sheets have been enlarged here for illustrative purposes and do not represent the true size/position and number of sheets in the myocardium.

The following is a detailed description of the different stages in the proposed model:

1.   Normal Phase

Figure 20A shows a cross-section of the LV of the normal heart before being subjected to pressure overload. The sheet size and numbers in Figure 20A represent those that are present in a healthy, working myocardium, free of any disease. This is purely a diagrammatic representation and in no way represents the true LV cross-section.
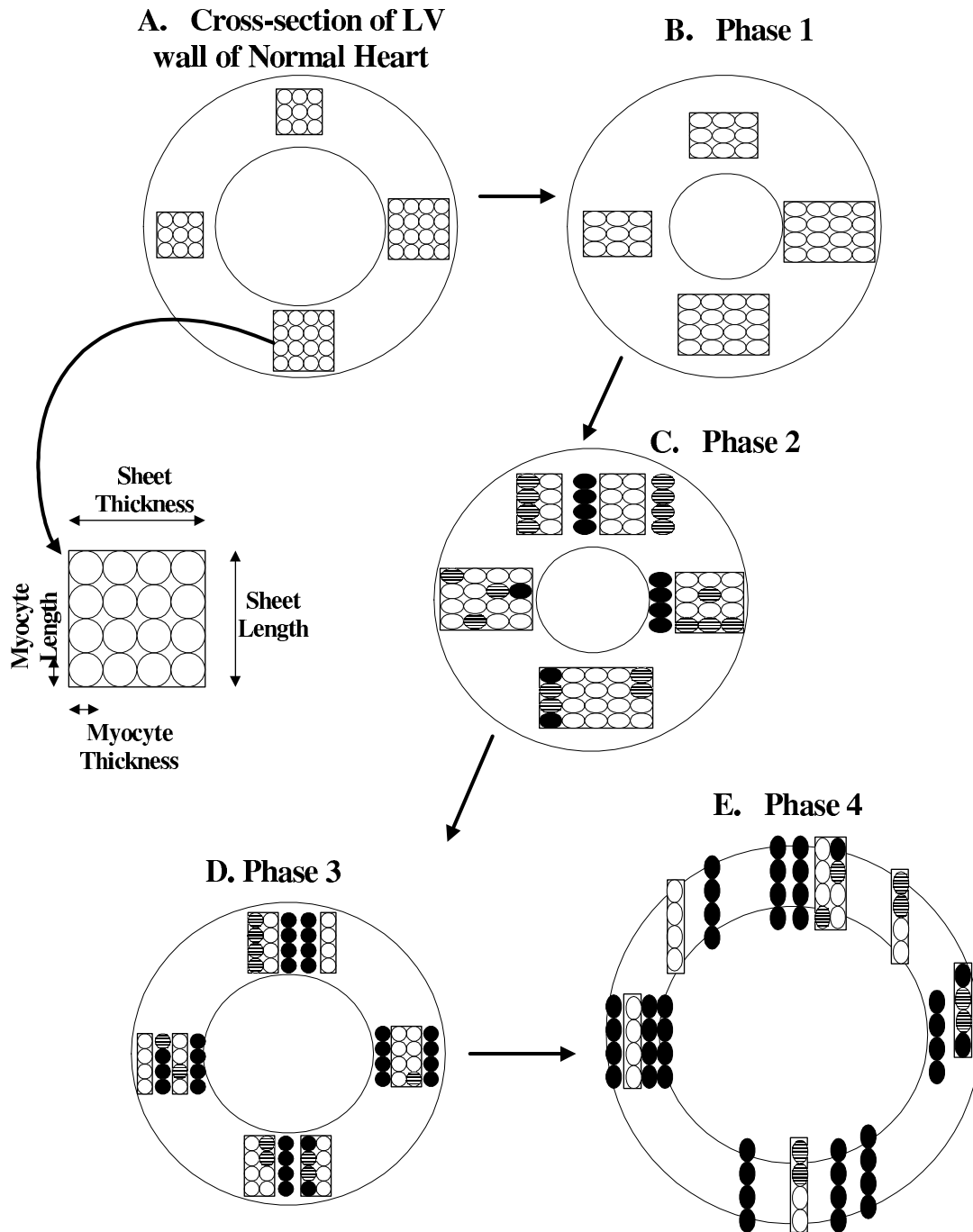
Fig. 20. The Proposed Growth Model; Note: A. Normal LV Cross-section; B. Phase 1: Mild Pressure Overload; C. Phase 2: Excessive Pressure Overload; D. Phase 3: Transitional Eutrophy; E. Phase 4: Dilated Hypertrophy; The rectangles represent cross-section of individual sheets and the circles inside them represent myocytes. Observe the change in thickness of myocytes and sheets as the heart progresses to failure. Black ellipses refer to dead myocytes and the patterned ellipses refer to newly proliferated myocytes

2. Phase I: Mild Pressure Overload

When this healthy heart is now subjected to pressure overload, as per Grossman's theory (27), the increase in the peak systolic stress leads to parallel replication of sarcomeres, resulting in thickening of individual myocytes. This is the initial stage of pressure overload (few weeks in animals; duration may vary in humans) where the myocardium has started making adjustments at the myocyte level to accomodate the increased mechanical stress. Figure 20B shows that the thickening of individual myocytes results in an increase in the thickness of the individual sheet. These developments lead to an increase in the wall thickness as seen in Figure 20B and increased thickness of wall to radius ratio. Note that at this stage there are no new myocytes/sheets formed and the length of the myocytes remains unchanged. This initial phase of pressure-overload results in concentric hypertrophy that compensates the additional workload. Hence, this is a well-compensated phase of hypertrophy where the heart is still functioning as normal. Highlights of Phase 1 are:

1. Well-compensated state of pressure overload; wall thickness increases.

2. Sheets get thicker than normal as myocytes get thicker.

3. Number of sheets remains same as original number.

4. No proliferation or loss of myocytes and sheets.
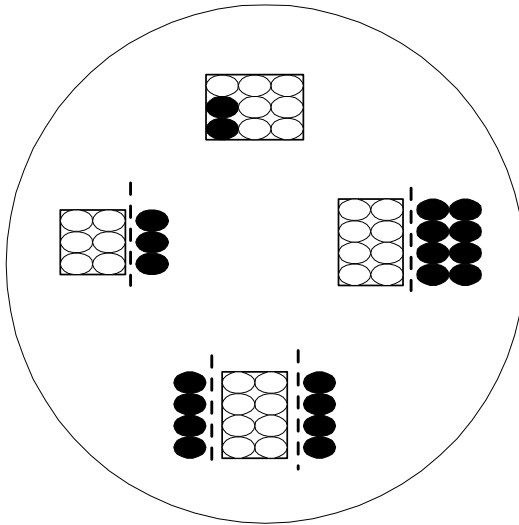
3. Phase II: Excessive Pressure Overload

The compensation in the initial phase continues for a long duration of time (could range from weeks in animals to years in humans) during which it seems that the heart continues to function normally. Figure 20C represents the excessive pressure overload phase. Here, the heart has been subjected to pressure overload for a long duration of

time. Yet, as the pressure overload continues, several changes start occurring at the myocyte level.
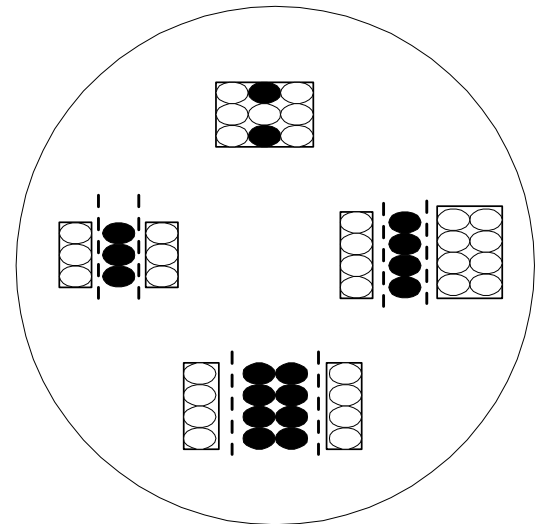
Hence, we propose that at this stage of overload, two situations exist simultaneously: The sustained mechanical stress/strain results in the proliferation of myocytes. The new myocytes formed by mitosis may or may not become part of the original sheet or may join a group of myocytes to form a new sheet. How this sheet formation occurs is still unknown. This would cause the sheet numbers to increase. Another possibility of the effect of myocyte proliferation is that it may result in the thickening of existing sheets and subsequently result in no change in sheet numbers. Alongside, myocyte loss begins concurrently due to apoptosis. Apoptosis also serves to maintain tissue integrity. As seen in Figure 20C, the sheet numbers increase because of the increase in myocyte numbers. Sheet numbers may also increase because of death of a whole column of myocytes which causes the sheet to split into two. If the newly formed myocytes join the original sheet, sheet numbers may remain constant. The black ellipses in Figure 20C, D and E refer to myocytes lost by apoptosis/necrosis. The individual myocytes are still as thick as in the initial phase of overload but the thickness of the sheets will vary. At this phase, the proliferation of myocytes is much greater than apoptosis, hence the number of new myocytes formed are much greater than the number of myocytes lost.

Thus, the sheet thickness will depend on the number of new myocytes that are added to it. Sheet thickness will also depend on which myocytes in an individual sheet are lost. If a whole column of myocytes is lost as shown in Figure 21 then sheet thickness will reduce. Similarly, sheet numbers will depend on the ability of new myocytes to group into sheets (or maybe join existing sheets), as well as the mechanism of myocyte loss which might cause splitting of sheets into two hence increase in sheet numbers. Which myocytes in a sheet are lost when remodeling first

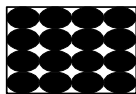Fig. 21. Mechanisms of Myocyte Death in a Sheet for Phase 2; Note: The black ellipses refer to dead myocytes. The dotted line signifies a split in the sheet due to the death of the myocytes. These mechanisms of myocyte death also apply to Phase 3 and Phase 4

begins; which part of the sheet is hit first when the remodeling begins??? This is unknown at this stage. Figure 21 shows that myocyte death in a sheet could be initiated in one of four probable situations that could happen at this stage. The dotted line signifies the splitting up of a sheet due to loss of myocytes. This can happen in one of 4 ways as explained in Figure 21A, B and C and D.

1. Figure 21A represents **myocyte death initiated at the sheet ends.** If this is the mechanism then only the ends would die out first so the number of sheets would still remain the same. The thickness of the sheets would be much reduced though. Another possibility though is that although the myocytes die out, the sheet may not split which may cause the sheet numbers to stay the same but thickness of sheets to increase. Yet since apoptosis involves total cleanup of cell debris we are inclined to believe that cell death at the ends of the sheet will result in reduced sheet thickness.

2. Figure 21B represents **myocyte death initiated in the middle of the sheet.** If this is the way by which the remodeling starts to occur then, the number of sheets would increase very steeply at this stage since every sheet is splitting into two much thinner sheets. Newer myocytes formed may or may not be part of the existing sheets. Hence, this mechanism of remodeling would cause the highest increase in the number of sheets and also result in the thinnest sheets, probably thinner than the original sheet thickness. Again, the possibility exists that some myocytes in the middle of a sheet die out and the sheet does not split up in which case the sheet thickness would be very high due to high loss of myocytes.

3. Figure 21C represents **all myocytes in a sheet dying together.** This mechanism of remodeling entails that all the myocytes of a single sheet die together.

This would mean a reduced number of sheets (fewer than parts A and B), though proliferation would add some new sheets so the number of sheets may not differ significantly from the original. It would also mean no significant change occurs in sheet thickness. Hence sheet thickness would still remain much higher than compared to original sheet thickness due to the thickened myocytes of Phase 2.

4. Figure 21D represents **myocytes dying randomly.** This method is a mix of parts A, B and C and would result in some sheets splitting into two, some staying the same, and some dying altogether. Hence it is hard to predict the sheet numbers and thickness if the remodeling is random.

The above four cases have one thing in common: the assumption that the same number of new myocytes may be added to the split sheets and/or to the existing unsplit sheets in each case. Also, since remodeling is a continuous process each stage described above is only a starting point for myocyte loss which could spread to the surrounding cells depending on stress and strain experienced by the cells. We do not have data for this particular stage of hypertrophy. Yet, based on the above descriptions, we surmise that at this stage, there is a steep increase in the number of sheets as compared to Phase 1 yet the sheet thickness will depend on addition of new myocytes to existing sheets as well as preferred mechanism of myocyte loss as shown in Figure 21. Whether Figure 21A, B C or D are the actual mechanisms that cause the increase in sheet numbers is unknown. Hence, although this stage is still compensated by the increased wall thickness, it is actually precursor to decompensation as it is the phase "just prior" to decompensation. Highlights of Phase 2 are:

1. Compensated State of pressure overload just prior to decompensation; wall still thickened.

2. Sustained stress/strain gives rise to new myocytes.

3. Simultaneously, myocyte loss due to apoptosis occurs.

4. Proliferation of myocytes is greater than loss of myocytes.

5. Number of sheets may increase due to splitting up of existing sheets caused by dying myocytes and also new myocytes forming new sheets; number of sheets may also remain constant if the newly formed myocytes join the existing sheets.

6. Myocytes still thick; sheet thickness will vary depending on new myocytes added to existing sheets and mechanism of myocyte death.

4. Phase III: Transitional Eutrophy (Decompensation Starts)

This is the phase when the myocardium is unable to keep up with the increased afterload imposed by the sustained pressure overload. Hence at this stage, all the adaptive and compensatory mechanisms break down and the thickened wall now slowly begins to thin out. In the process of going from a thickened wall to a thinner one, the heart will retrace its original shape and size as shown in Figure 20D. At this particular stage the size and shape of the heart will resemble the normal heart but it has undergone a totally different mechanical history from a normal heart. Hence this stage is called "Transitional Eutrophy".

At this phase, as seen in Figure 20D, the thickened myocytes will regain their original shape and size. Proliferation of myocytes continues at this stage, yet decompensation results in a substantial loss of myocytes; hence loss of myocytes is much greater than proliferation of myocytes. The number of sheets at this stage is still high because although there is some proliferation, rate of lost myocytes is high hence possibility of sheets splitting up is also very high. The thickness of the sheets is less than the original thickness since although the individual myocytes are of the same shape and size as the original, a number of myocytes of an individual sheet could be

lost due to the rampant loss of myocytes. As explained in Phase 2, the mechanism of myocyte loss plays a role in determining the thickness of the sheets. Our data that was collected at this stage is in agreement with this theory as there was a significant increase in sheet numbers at this stage along with a significant reduction in sheet thickness. These results show that myocyte death was initiated most probably by case Figure 21B or with less probability Figure 21A since both of these cases, especially Figure 21B would result in increased sheet numbers and decreased sheet thickness. Figure 21A may result in decreased sheet thickness but the sheet numbers would still remain the same as the original or just slightly lower which was not what was observed. Figure 21C is also not a probability as this case would result in similar sheet thickness to the original which does not match with our observed data. Figure 21D is a possibility if there is no set pattern to the remodeling mechanism hence resulting in random remodeling. Yet, we think this is a remote possibility due to the similar increases of sheet numbers and reductions of sheet thickness obtained at all four quarters of the septae which suggest a distinct trend. Highlights of Phase 3 are:

1. Loss of myocytes is greater than proliferation of myocytes.

2. Decompensation begins; wall starts thinning out.

3. Myocytes return to normal shape and size.

4. Sheets are much thinner than original and also very high in number due to higher apoptosis increasing the probability of split sheets.

5. Phase IV: Dilated Hypertrophy (Severe Decompensation)

As the decompensation continues, the wall of the heart starts dilating even more and starts thinning out leading to chamber enlargement as shown in Figure 20E.

This happens because the loss of myocytes is significantly greater than the myocyte proliferation. Also, myocyte death by apoptosis causes the side-to-side mural slippage of the myocytes within the wall resulting in wall thinning and subsequent reduction in wall thickness. Concurrently, the existing myocytes are themselves getting longer because of the series replication of sarcomeres leading to increase in the length of the individual myocytes hence also length of the sheets. We do not have data for this phase of hypertrophy too hence we can only predict what can occur at this stage on the basis of our results of Phase 3. Myocyte numbers hence sheet numbers will be the lowest in this phase due to the significant loss of myocytes and slower cell regeneration. Although the thickness of the myocytes will not change much, the sheet thickness will be reduced even more than at Phase 3 because of the significant reduction in myocyte numbers. Ultimately, myocyte death and the mural slippage of myocytes could create an irreversible state causing failure in the myocardium. Highlights of Phase 4 are:

1. Loss of myocytes is much greater than proliferation of myocytes.

2. Severe decompensation; excessive wall thinning and chamber dilation.

3. Myocytes get longer hence sheets get longer.

4. Sheets are the thinnest here but the least in number due to extremely high numbers of myocyte death.

6. Discussion about Model

This model is a pictorial representation of sheet morphology changes as the heart progresses toward hypertrophy. The predictions of sheet numbers and thickness are based on past research on myocyte behavior in overload conditions as well as the data obtained from the present study. Past research has shown that a short-term or

gradual increase in pressure overload involves only myocyte hypertrophy (45) whereas a sustained increase in workload as happens in long-term pressure overload involves myocyte proliferation (33, 11, 46). It has also been shown that myocyte loss by apoptosis occurs in hypertension (39). These theories about the myocyte have been employed in the proposed model and extended to the study of sheet probable sheet morphology in these hypertrophied states.

At this point, it is important to mention that we have not considered the details of myocyte death by apoptosis, necrosis etc. Hence whenever we mention myocyte loss it is a generalization and encompasses all forms of cell death. Similarly, mechanisms of myocyte proliferation have not been dealt with as well. Also, we are aware that myocyte loss results in the underestimation of myocyte proliferation whereas myocyte proliferation leads to an underestimation of the magnitude of myocyte death, due to the co-existence of both the situations at the same time which may lead to an inaccurate representation of myocyte and sheet numbers. This model is important because it is a vital tool in the study of comparison of sheet behavior (especially comparison of sheet numbers and thickness) from healthy and diseased hearts. The model helps to know what sheet behavior one can expect if a study of diseased hearts in any of the above phases is conducted thus paving the way for future focussed research in this area.

CHAPTER VI

CONCLUSIONS AND FUTURE RECOMMENDATIONS

A. Conclusions

The goals of this study were to understand the differences in the microstructure of normals heart septate versus hearts that are progressing toward heart failure. This work gave us a good insight into the differences in structure of both groups of hearts based on fiber angle orientation, sheet angle orientation, uniformity index, number of sheets and thickness of sheets. In conclusion, using a tissue processing method that directly and efficiently measured myolaminar morphology we have analyzed the fiber and sheet structure in a rat model of pressure overload hypertrophy transitioning to dilated heart failure. To our knowledge this is the first comparative study of the myolaminar microstructure of normal hearts versus hearts undergoing hypertrophy. The following information was revealed by this study:

1. A new phase of hypertrophy that lies in between the stages of concentric hypertrophy and dilated hypertrophy was revealed and coined as "Transitional Eutrophy". It was found that at this stage of hypertrophy, the heart being in transition from having a thickened wall to a thinner one, has a similar shape and size as the control group of hearts which were not subjected to the pressure overload.

2. At this stage of hypertrophy, it was found that the septae of the pressure overloaded HS group of hearts showed an almost three-fold increase in sheet numbers.

3. Concurrently, the HS group of hearts also showed a significant decrease in sheet

thickness.

4. In the overloaded hearts, the fiber angles increased significantly at all depths of the septum except at TQ3. Total span of the fiber angle remained constant ($108°$).

5. The sheet angle differences were not significant in the HS group.

6. Uniformity Index which signified uniformity in orientation of sheet angles, varied transmurally in the LS group of hearts; in the HS group, the uniformity index was negative indicating that the sheets were oriented in the negative direction and that transmural variations reduced as hearts undergo hypertrophy.

7. A model that predicts the changes in sheet morphology as the heart transitions to failure under conditions of sustained pressure overload was proposed.

8. The proposed model also predicts the initial mechanisms of myocyte death per sheet as the heart progresses to failure. The model can be used as a useful tool to predict sheet behavior at various stages of overload prior to failure.

B. Limitations of the Study

The observations of sheet morphology are limited to the interventricular septum of rats. We are aware that there can be a significant variation in sheet structure in different regions of the heart as well as a variation based on different species as well. Caution should be exercised while extrapolating these results to other regions of the heart and also other species. Such a thorough analysis though is beyond the scope of this study.

C.   Future Work

Based on the results obtained from the present study, the following work could be carried out in the near future:

1. Conduct a comparative study of the microstructure involving measurement of fiber angles, sheet angles, uniformity index, sheet numbers, lengths and thickness of normal hearts versus hearts undergoing concentric hypertrophy at the initial phase (Phase 1) and verify the predictions of the model for sheet numbers, lengths and thickness. It will also be very useful to take blood pressure and heart rate measurements of the rats in both groups. 2-D echocardiography could be used to measure in vivo systolic and diastolic chamber diameter and wall thickness. LV and RV pressure, LV and RV peak systolic pressure and LV end-diastolic pressure could be calculated. Wall stress could be calculated using echo and LV pressure data. Number of myocytes present per sheet would be another useful parameter to measure as it would validate the model's predictions of fewer myocytes resulting in thinner sheets.

2. Repeat the above microstructure study at the severe pressure-overload hypertrophy phase (Phase 2) and also at the dilated hypertrophy phase (Phase 4).

3. Diffusion tensor MRI is increasingly becoming popular as a valuable tool for the study of the microstructure rapidly and non-invasively. This methodology may be employed and tested for measurement of fiber and sheet angles in future experiments. Phase contrast MRI could be used to acquire strain rate images of the myocardium.

4. Measure the three major sheet strains: sheet extensions, sheet shear and sheet normal thickening and also the cross-fiber shear at diastole when the wall thins

in both groups in the above experiments.

5. It is still unclear as to what sheet functions can be defined as normal and what can be classified as abnormal. Clear criteria by which we could distinguish sheet function in normal hearts versus that in diseased heart is extremely vital to the advancement of this research. Larger numbers of healthy and diseased subjects of various species will have to be studied for this.

6. The Spontaneously Hypertensive Rat (SHR) is a widely used and popular model for studying hypertension in an animal model. The above future studies could incorporate some rats of this type. This would allow a three-way comparison and also help prove whether the observations of our study are true only for one particular animal model (Dahl salt-sensitive rat) or are applicable to multiple animal models as well.

7. Excessive volume overload hypertrophy would also eventually lead to heart failure. A study where subjects would be subjected to excessive volume overload would be a very useful one as it would allow for a comparison of the present study with a completely different source of overload but with the same detrimental effects. It would be interesting to see how different fiber and sheet morphology and mechanics are when the sources of overload are vastly different.

REFERENCES

1. **Anversa P.** Myocyte apoptosis and heart failure. *Eur Heart J* 19(3): 359-60, 1998.

2. **Anversa P, Annarosa L, Kajstura J and Bernardo Nadal-Ginard.** Myocyte growth and cardiac repair. *J Mol Cell Cardiol* 34: 91-105, 2002.

3. **Anversa P, Kajstura J.** Ventricular myocytes are not terminally differentiated in the adult mammalian heart. *Circ Res* 83: 1-14, 1998.

4. **Anversa P, Leri A, Beltrami CA, Guerra A, Kajstura J.** Myocyte death and growth in the failing heart. *Lab Invest* 78: 767-786, 1998.

5. **Anversa P, Loud AV, Giacomelli F, Wiener J.** Absolute morphometric study of myocardial hypertrophy in experimental hypertension. II. Ultrastructure of myocytes and interstitium. *Lab Invest* 38(5): 597-609, 1978.

6. **Anversa P, Olivetti G.** Cellular basis of physiologic and pathologic myocardial growth. In *Handbook of Physiology. The Cardiovascular System. The Heart.* New York: Oxford University Press, 2001, sect. 2, vol. 1, 2001, p. E.

7. **Anversa P, Olivetti G, Leri A, Liu Y, Kajstura J.** Myocyte death and remodeling. *Curr Opin Nephrol Hypertens* 6: 169-176, 1997.

8. **Anversa P, Palackal T, Sonnenblick EH, Olivetti G, Capasso JM.** Hypertensive cardiomyopathy: myocyte nuceli hyperplasia in the mammalian heart. *J Clin Invest* 85: 994-997, 1990.

9. **Arts T, Costa KD, Covell JW, McCulloch AD.** Relating myocardial laminar architecture to shear strain and muscle fiber orientation. *Am J Physiol* 280(5): H2222-9, 2001.

10. **Ashikaga H, Criscione JC, Omens JH, Covell JW, Ingels NB Jr.** Transmural left ventricular mechanics underlying torsional recoil during relaxation. *Am J Physiol* 286(2): H640-7, 2004.

11. **Beltrami AP, Urbanek K, Kajstura J, Yan SM, Finato N, Bussani R, Nadal-Ginard B, Silvestri E, Leri A, Beltrami CA, Anversa P.** Evidence that human cardiac myocytes divide after infarction *N Engl J Med* 344: 1750-1757, 2001.

12. **Berne RM, Levy MN.** *Cardiovascular Physiology.* St. Louis: Mosby, 2001, p. 55-81.

13. **Capasso JM, Palackal T, Olivetti G, Anversa P.** Left ventricular failure induced by long-term hypertension in rats. *Circ Res* 66(5): 1400-12, 1990.

14. **Caulfield, JB, Borg TK.** The collagen network of the heart. *Lab Invest* 40(3): 364-72, 1979.

15. **Chen J, Liu W, Zhang H, Lacy L, Yang X, Song SK, Wickline SA, Yu X.** Regional ventricular wall thickening reflects changes in cardiac fiber and sheet structure during contraction: quantification with diffusion tensor MRI. *Am J Physiol Heart Circ Physiol* 289(5): H1898-907, 2005.

16. **Cheng W, Reiss K, Li P, Chun MJ, Kajstura J, Olivetti G, Anversa P.** Aging does not affect the activation of the myocyte insulin-like growth factor-1

autocrine system after infarction and ventricular failure in Fisher 344 rats. *Circ Res*, 78: 536-546, 1996.

17. **Conrad CH, Brooks WW, Robinson KG and Bing OHL.** Impaired myocardial function in spontaneously hypertensive rats with heart failure. *Am J Physiol* 260: H136145, 1991.

18. **Costa KD, Takayama Y, McCulloch AD, Covell JW.** Laminar fiber architecture and three-dimensional systolic mechanics in canine ventricular myocardium. *Am J Physiol* 276(2 Pt 2): H595-607, 1999.

19. **Cotran RS, Kumar V, Collins T, Robbins SL.** *Robbins Pathologic Basis of Disease.* Philadelphia: W.B. Saunders Company, 1999, p. 546-550.

20. **Diez J, Fortuno MA, Ravassa S.** Apoptosis in hypertensive heart disease. *Curr Opinion in Cardiol* 13: 317-325, 1998.

21. **Dou J, Tseng WY, Reese TG, Wedeen VJ.** Combined diffusion and strain MRI reveals structure and function of human myocardial laminar sheets in vivo. *Magn Reson Med* 50(1): 107-13, 2003.

22. **Fujiwara H, Fujiwara T, Hamashima Y, Kawai C.** Number and size of myocytes, amount of interstitial space and extent of disarray of the hearts in patients with systemic hypertension and asymmetric septal hypertrophy. *Jpn Circ J* 49(4): 406-14, 1985.

23. **Geerts L, Bovendeerd P, Nicolay K, Arts T.** Characterization of the normal cardiac myofiber field in goat measured with MR-diffusion tensor imaging. *Am J Physiol Heart Circ Physiol* 283: H139-H145, 2002.

24. **Gerdes AM and Capasso JM.** Structural remodeling and mechanical dysfunction of cardiac myocytes in heart failure. *J Mol Cell Cardiol* 27: 849-856, 1995.

25. **Grajek S, Lesiak M, Pyda M, Zajac M, Paradowski S, Kaczmarek E.** Hypertrophy or hyperplasia in cardiac muscle: postmortem human morphometric study. *Eur Heart J* 14: 40-47, 1993.

26. **Grossman W.** Cardiac hypertrophy: useful adaptation or pathologic process. *Am J Med* 69(4): 576-584, 1980.

27. **Grossman W, Jones D and Mclaurin L.** Wall stress and patterns of hypertrophy in the human left ventricle. *J Clin Invest* 56: H56-64, 1975.

28. **Guerra A, Leri A, Wang X, Finato N, Di Loreto C, Beltrami CA, Kajstura J, Anversa P.** Myocyte death in the failing human heart is gender dependent. *Circ Res* 85: 856-66, 1999.

29. **Harrington KB, Rodriguez F, Cheng A, Langer F, Ashikaga H, Daughters GT, Criscione JC, Ingels NB, Miller DC.** Direct measurement of transmural laminar architecture in the anterolateral wall of the ovine left ventricle: new implications for wall thickening mechanics. *Am J Physiol* 288(3): H1324-30, 2005.

30. **Hess OM, Ritter M, Schneider J, Grimm J, Turina M, Krayenbuehl HP.** Diastolic stiffness and myocardial structure in aortic valve disease before and after valve replacement. *Circulation* 69(5): 855-65, 1984.

31. **Humphrey JD.** *Cardiovascular Solid Mechanics.* New York: Springer-Verlag, 2002, p. 601- 617.

32. **Inoko M, Kihara Y, Morii I, Fujiwara H, Sasayama S.** Transition from compensatory hypertrophy to dilated, failing left ventricles in Dahl salt-sensitive rats. *Am J Physiol* 267(2 Pt 2), H2471-82, 1994.

33. **Kajstura J, Leri A, Finato N, Di Loreto C, Beltrami CA, Anversa P.** Myocyte proliferation in end-stage cardiac failure in humans. *Proc Natl Acad Sci USA* 95: 8801-8805, 1998.

34. **LeGrice IJ, Hunter PJ, Smaill BH.** Laminar structure of the heart: a mathematical model. *Am J Physiol* 272(5 Pt 2): H2466-76, 1997.

35. **LeGrice IJ, Smaill BH, Chai LZ, Edgar SG, Gavin JB, Hunter PJ.** Laminar structure of the heart: ventricular myocyte arrangement and connective tissue architecture in the dog. *Am J Physiol* 269(2 Pt 2): H571-82, 1995.

36. **LeGrice IJ, Takayama Y, Covell JW.** Transverse shear along myocardial cleavage planes provides a mechanism for normal systolic wall thickening. *Cir Res* 77(1): 182-93, 1995.

37. **Levick JR.** *An Introduction to Cardiovascular Physiology.* London: Arnold Publishers, 2003.

38. **Levy D, Larson MG, Varsan RS, Kannel WB, Ho KKL.** The progression from hypertension to congestive heart failure. *JAMA* 275: 1557-1562, 1996.

39. **Li Z, Bing OHL, Long X, Robinson KG, Lakatta EG.** Increased cardiomyocyte apoptosis during the transition to heart failure in the spontaneously hypertensive rat. *Am J Physiol* 272: H2313-H2319, 1997.

40. **Linzbach AJ.** Heart failure from the point of view of quantitative anatomy", *Am J Cardiol* 5: 370-382, 1960.

41. **Litwin SE, Litwin CM, Raya TE, Warner AL, and Goldman S.** Contractility and stiffness of noninfarctedyocardium after coronary ligation in rats. Effects of chronic angiotensin converting enzyme inhibition. *Circ Res* 83: 1028-1037, 1991.

42. **Lunkenheimer PP, Redman K, Anderson RH.** The architecture of the ventricular mass and its functional implications for organ-preserving surgery. *Eur J Cardiothorac Surg* 27(2): 183-90, 2005.

43. **Mirsky I, Pfeffer JM, Pfeffer MA, Braunwald E.** The contractile state as the major determinant in the evolution of left ventricular dysfunction in the spontaneously hypertensive rat. *Circ Res* 53: 767-78, 1983.

44. **Nielsen PM, Le Grice IJ, Smaill BH, Hunter PJ.** Mathematical model of geometry and fibrous structure of the heart. *Am J Physiol* 260(4 Pt 2): H1365-78, 1991.

45. **Olivetti G, Melissari M, Balbi T, Quani F, Cigola E, Sonnenblick EH, Anversa P.** Myocyte cellular hypertrophy is responsible for ventricular remodeling in the hypertrophied heart of middle aged individuals in the absence of cardiac failure. *Cardiovasc Res* 28(8): 1199-208, 1994.

46. **Olivetti G, Melissari M, Balbi T, Quani F, Sonnenblick EH, Anversa P.** Myocyte nuclear and possible cellular hyperplasia contribute to ventricular remodeling in the hypertrophic senescent heart in humans. *J Am Coll Cardiol* 24: 140-49, 1994.

47. **Olivetti G, Ricci R, Anversa P.** Hyperplasia of myocyte nuclei in long-term cardiac hypertrophy in rats. *J Clin Invest* 80: 1818-1821, 1987.

48. **Olivetti G, Ricci R, Lagrasta C, Maniga E.** Cellular basis of wall remodeling in long-term pressure overload-induced right ventricular hypertrophy in rats. *Circ Res* 63: 648-657, 1988.

49. **Omens JH.** Stress and strain as regulators of myocardial growth. *Prog Biophys Mol Biol* 69: H559-572, 1998.

50. **Peterson KL.** Pressure overload hypertrophy and congestive heart failure where is the achilles heel. *J Am Coll Cardiol* 39(4): 672-675, 2002.

51. **Peterson KL, Tsuji J, Johnson A, DiDonna J, LeWinter M.** Diastolic left ventricular pressure-volume and stress-strain relations in patients with valvular aortic stenosis and left ventricular hypertrophy. *Circulation* 58: 77-89, 1978.

52. **Pfeffer MA, Pfeffer JM, Fishbein MC, Fletcher PJ, Spadaro J, Kloner RA, and Braunwald E.** Myocardial infarct size and ventricular function in rats. *Circ Res* 44: 503-512, 1979.

53. **Randhawa AK, and Singal PK.** Pressure overload-induced cardiac hypertrophy with and without dilation. *J Am Coll Cardiol* 20(7): 1569-75, 1992.

54. **Reiss K, Kajstura J, Zhang X, Li P, Szoke E, Olivetti G,Anversa P.** Acute myocardial infarction leads to the upregulation of the IGF-1 autocrine system, DNA replication, and nuclear mitotic divsion in the remaining viable cardiac myocytes. *Exp Cell Res* 213: 463-472, 1994.

55. **Ross J, Jr.** Afterload mismatch and preload reserve: a conceptual framework for the analysis of ventricular function. *Prog Cardiovasc Dis* 38: 255-64, 1976.

56. **Sandritter W, Adler CP.** Numerical hyperplasia in human heart hypertrophy. *Experimentia* 27: 1435-37, 1971.

57. **Sasayama S, Ross J Jr, Franklin D, Bloor CM, Bishop S, Dilley RB.** Adaptations of the left ventricle to chronic pressure overload. *Circ Res* 38(3): 172-8, 1976.

58. **Serizawa T, Mirsky I, Grossman W and Carabello B.A.** Diastolic myocardial stiffness in gradually developing left ventricular hypertrophy in dog. *Am J Physiol* 242: H633-637, 1982.

59. **Siri FM, Krueger J, Nordin C, Ming Z and Aranson RS.** Depressed intracellular calcium transients and contraction in myocytes from hypertrophied and failing guinea pig hearts. *Am J Physiol* 261: H514530, 1991.

60. **Siri FM, Nordin C, Factor SM, Sonnenblick E, Aronson R.** Compensatory hypertrophy and failure in gradual pressure-overloaded guinea pig heart. *J Am Coll Cardiol*, 257(3 Pt 2): H1016-24, 1989.

61. **Spotnitz HM, Spotnitz WD, Cottrell TS, Spiro D, Sonnenblick EH.** Cellular basis for volume related wall thickness changes in the rat left ventricle. *Magn Reson Med* 6(4): 317-31, 1974.

62. **Streeter DD Jr.** Gross morphology and fiber geometry of the heart. In *Handbook of Physiology. The Cardiovascular System. The Heart.* Bethesda, MD: Am. Physiol Soc., 1979, sect. 2, vol. I, chapt.4, p. 61-112.

63. **Streeter DD Jr, Spotnitz HM, Patel DP, Ross J Jr, Sonnenblick EH.** Fiber orientation in the canine left ventricle during diastole and systole. *Circ Res* 24(3): H339-47, 1969.

64. **Takayama Y, Costa KD and Covell JW**. Contribution of laminar myofiber architecture to load-dependent changes in mechanics of LV myocardium. *Am J*

Physiol Heart Circ Physiol 282: H1510-H1520, 2002.

65. **Vaux DL.** Toward an understanding of the molecular mechanisms of physiological cell death. *Proc Natl Acad Sci USA* 90: 786-789, 1993.

66. **Wagoner LE, Walsh RA.** The cellular pathophysiology of progression to heart failure. *Curr Opin Cardiol* 11: 237-244, 1996.

67. **Waldman LK, Nosan D, Villareal F and Covell JW.** Relation between transmural deformation and local myofiber direction in canine left ventricle. *Circ Res* 63(3): 550-62, 1988.

68. **Weber KT.** Extracellular matrix remodeling in heart failure: a role for de novo angiotensin II generation. *Circulation* 96: 4065-4082, 1997.

69. **Weber KT.** Fibrosis and hypertensive heart disease. *Curr Opin Cardiol* 15: 264-272, 2000.

70. **Weber KT.** Fibrosis in hypertensive heart disease: focus on cardiac fibroblasts. *J Hypertens* 22(1): 47-50, 2004.

71. **Young AA, Legrice IJ, Young MA, Smaill BH.** Extended confocal microscopy of myocardial laminae and collagen network. *J Microsc* 192(Pt 2): 139-50, 1998.

72. **Zimmerman SD, Criscione J, Covell JW.** Remodeling in myocardium adjacent to an infarction in the pig left ventricle. *Am J Physiol Heart Circ Physiol* 287(6): H2697-704, 2004.

VITA

Bharati Krishna Hegde was born in Sirsi, Karnataka, India. She received her B.E. degree in Electronics Engineering from the Vishwakarma Institute of Technology, University of Pune, India in 1999. She worked as a Programmer Analyst with Cognizant Technology Solutions, Pune, India from July 1999 to July 2000. She joined the Department of Biomedical Engineering at Texas A&M University in August 2000 to pursue her Master's degree and received her M.S. degree in Biomedical Engineering in May 2003. She started to pursue her Ph.D degree in Biomedical Engineering in August 2003 and received her Ph.D degree in August 2006. Her permanent address is:

Bharati Krishna Hegde

A-1, 19, Solace Park

B.T. Kawade Road, Ghorpadi

Pune-411013, Maharashtra, India